Master's thesis

NTNU
Norwegian University of Science and Technology
Faculty of Natural Sciences
Department of Physics

Jonas Lidal

Photon-assisted Landau-Zener transitions in driven few-level systems

Master's thesis in Physics
Supervisor: Jeroen Danon
May 2019

NTNU
Kunnskap for en bedre verden

Jonas Lidal

Photon-assisted Landau-Zener transitions in driven few-level systems

Master's thesis in Physics
Supervisor: Jeroen Danon
May 2019

Norwegian University of Science and Technology
Faculty of Natural Sciences
Department of Physics

NTNU
Kunnskap for en bedre verden

Abstract

In this thesis we investigate photon-assisted Landau-Zener transitions in driven few-level systems. We both treat the driving field semi-classically (as a time-dependent parameter in the Hamiltonian) and fully quantum-mechanically (as a photon field). We first present the basic theory of Landau-Zener transitions as well as strong and weak semi-classical driving. These ingredients are then used to propose two methods using NV-centers in diamonds as magnetometers. One inspired by Landau-Zener-Stückelberg intererometry, using photon assisted Landau-Zener transitions, and another using "indirect" Rabi driving, where we obtain Rabi oscillations between two levels by driving a third level. The viability of both methods is discussed, where the latter is pointed out as the most promising. We then start treating the driving quantum mechanically, starting with presenting the basic theory of two-level systems coupled to a single photon mode, before introducing Landau-Zener transitions into such models. We apply what we see here to manipulate coherent states and a superposition of these states, known as Schrödinger cat states. Ultimately, presenting a new method for creating such cat states using photon assisted Landau-Zener transitions.

Samandrag

I denne avhandlinga utforskar me Landau-Zener overgangar i drivne få-nivå system. Me behandlar drivingsfeltet både semi-klassisk (som ein tidsavhengig parameter i Hamilton operatoren) og heilt kvantemekanisk (som eit fotonfelt). Me presentere først den grunnleggande teorien bak Landau-Zener overgangar samt sterk og svak semi-klassisk driving. Me bruker så det me har presentert til å føreslå to metodar for måling av magnetfelt ved bruk av NV-senter i diamantar. Ein er inspirert av Landau-Zener-Stückleberg interfermetri, der foton-assistert Landau-Zener overgangar vert tatt i bruk, medan den andre brukar indirekte Rabi svingingar. Kor brukbare desse metodane er blir diskutert, der den andre av dei to metodane vert utpeikt som den mest lovande. Me startar så å behandle drivingsfeltet kvantemekanisk, der me byrjar med å presentere den grunnleggande teorien bak eit to-nivå system kopla til ein enkelt fotonmode, før me introduserer så Landau-Zener overgangar i modellar slik som dette. Me tek så dette i bruk til å manipulere koherente tilstandar og superposisjonar av desse, kjent som Schrödinger-kattetilstandar. Til slutt føreslår me ein ny metode for å lage slike kattetilstandar ved å bruke foton-assisterte Landau-Zener overgangar.

Preface

This thesis was written as a part of the physics masters program at the Norwegian University of Science and Technology (NTNU) during the fall of 2018 and the spring of 2019. I would like to thank assoc. prof. Jeroen Danon, who came up with the idea behind this thesis, for his insight, helpful comments and support during this year.

Table of Contents

Chapter 1

Introduction

Quantization is a fundamental principle of quantum mechanics. Physical systems can only exist in a discrete set of states (and superpositions thereof). The typical examples being particle in a box, or the electrons in an atom. In some systems only a few of these are important for the behaviour of the system, something we will refer to as a effective few-level system or just a few-level system (FLS). This can for instance be because the other states are of much higher energy than the typical energy of the system. Having systems like this, that are controllable, are interesting from fundamental point of view as it gives us a way to test and play around with the fundamental laws of quantum mechanics. In this thesis we are going to look at such FLSs and what happens when we introduce driving to these systems.

The case of FLSs are some of the simplest systems you can think of in quantum mechanics. Yet it is full of interesting physics, some of which we will investigate in this thesis. Effective FLS appear naturally in many settings. An example of a two-level system (TLS) is the states of an atom where there are only two relevant states, a ground state and a excited state [1, 2]. This being one of the systems that are not necessarily easy to control, but artificial atoms on the other hand are very controllable, single or multiple electrons can be trapped in artificial atoms, where they can be manipulated with great control [3, 4]. The spin of an electron is maybe the simplest example of a two level system. Without an external field the two states are degenerate, but in the presence of a magnetic field, the energy of the two states split. This is what is know as a Zeeman shift or Zeeman splitting [5]. One example of an effective three-level-system is the two electrons that form triplet states in a negatively charged nitrogen vacancy center (NV-center) in diamonds [6], a system we will look closer at in chapter 4.

Other than fundamental interest in the underlying physics, TLSs have also gathered quite a bit of attention the last decades for being possible candidates for the basic unit of quantum information, a qubit. Different TLSs have qualities that makes them suitable for different parts of a quantum computer. Some have excellent coherency properties making them good for storage, like the nuclear spin of Phosphorus-31, while others are easy to manipulate such as the electron spin [7]. Some systems are hybrids of these kinds of systems and have the advantage of being relatively good at both these properties. One example being NV-centers in Carbon-12 diamond with a single Carbon-13 near by, the electrons in the NV-centers are easily manipulated

and can be used to manipulate the stable spin of the carbon-13 nucleus [8, 9].

One fundamental question to ask when you have a controllable TLS is what would happen if you made the two levels cross? Keeping the coupling constant and driving the splitting linearly so that an avoided level crossing occurs is known as a Landau-Zener transition (LZT). The system then has a probability of staying in an adiabatic state after the crossing. LZTs have been investigated widely both theoretically (some examples being [10, 11]) and experimentally (an example being [12]). In this thesis we will look at such transitions in driven few-level system. We investigate both the case of classical driven systems and a fully quantum mechanical treatment of driving.

In chapter 2 we will start by reviewing the basics of Lanadu-Zener transitions, deriving the well known Landau-Zener formula, first using a complex path integral method and then looking at how it can be treated with time dependent perturbation theory. In chapter 3 we will look at classical driving in FLSs, leading to Rabi oscillations at resonance. First in the weak driving limit that we are used to, then we present an overview of the strong driving limit, where there are level crossings. In chapter 4 we will be using what we have presented in the previous two chapters in an application. Namely we will investigate classical driving in NV-centers in diamond as a potential high sensitivity magnetometer. Then in chapter 5 we will start to take the full quantum nature of the driving seriously, investigating the model of a photon mode coupled to a TLS. The introduction of this model will later allow us to investigate the effects of the photon-assisted Landau-Zener transition on the photon field. In chapter 6 we will investigating Landau-Zener transitions in the systems described in chapter 5. In chapter 7 we will be using what we have looked at to create and modify special light states. These light states have been found useful in many different areas of quantum physics, but are generally hard to produce with previously known methods.

1.1 Notation and convention

We establish some notation and convention that will be used throughout the thesis. All calculations will be done in natural units if nothing else is stated:

$$k_b = c = \hbar = 1 \tag{1.1}$$

Pauli matrices

We will use the Pauli matrices as shorthand, which are defined as:

$$\sigma_x = \begin{bmatrix} 0 & 1 \\ 1 & 0 \end{bmatrix}, \qquad \sigma_y = \begin{bmatrix} 0 & -i \\ i & 0 \end{bmatrix}, \qquad \sigma_z = \begin{bmatrix} 1 & 0 \\ 0 & -1 \end{bmatrix} \tag{1.2}$$

We will also be using the matrices:

$$\sigma_+ = \sigma_x + i\sigma_y = \begin{bmatrix} 0 & 2 \\ 0 & 0 \end{bmatrix}, \qquad \sigma_- = \sigma_x - i\sigma_y = \begin{bmatrix} 0 & 0 \\ 2 & 0 \end{bmatrix} \tag{1.3}$$

Chapter 2

The Landau-Zener problem

In this chapter we will look at what happens when we make two coupled levels cross. For the sake of simplicity we will keep it to a TLS in this chapter, generalizing somewhat in coming chapters. Crossing the levels by driving them linearly with a constant coupling is known as the the Landau-Zener problem, and is a well known problem in the fields of atomic and solid state physics. The problem was solved separately in publications by Lev Landau [13], Clarence Zener [14], Ernst Stückelberg [15] and Ettore Majorana [16] in 1932 and 1933.

If the two levels were not coupled, nothing would happen of course, the two levels are then just two separate one level systems which is trivial. The eigenstates during such a process is something we will call the diabatic basis. If they are coupled however, it is intuitive that something will happen when they cross where the coupling is at the same order as the level splitting. It is therefore not surprising that we get population transfer between the energy levels when the energy levels are close. But how big this transfer probability is, is not trivial. As we will see, the problem can be analytically solved, giving a simple expression for the transfer probability, the famous Landau-Zener formula.

2.1 Avoided level crossings

Let us start looking at the system by figuring out what the instantaneous eigenstates and energy eigenvalues of system are. The system is described in the diabatic basis by the Hamiltonian:

$$H = (\frac{1}{2}vt)\sigma_z + \delta\sigma_x \tag{2.1}$$

This describes a TLS where the splitting is vanishing at $t = 0$ closing in/separating with "speed" v, shown in figure 2.1. The diabatic basis are the eigenstates of σ_z, $\{|0\rangle, |1\rangle\}$, the energy eigenvalues of which are drawn as dashed lines in fig 2.1. Note that these are not eigenstates of the system if not $\delta = 0$. What we will call the adiabatic basis, $\{|E_+\rangle, |E_-\rangle\}$, the energy eigenvalue of which is drawn in full lines in 2.1). These are the instantaneous eigenstates of the Hamiltonian. We find the eigenvaules of these by solving the eigenvalue problem that is the

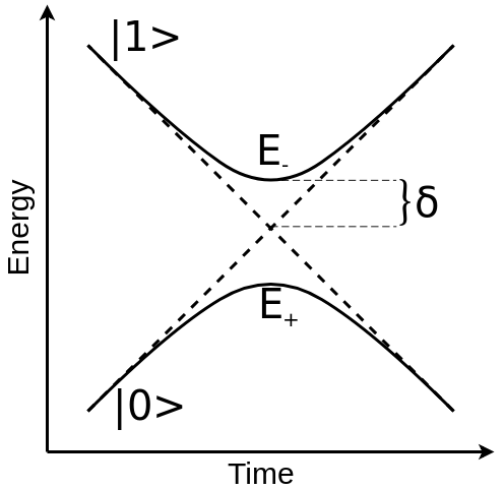

Figure 2.1: Schematic of an energy level diagram of an avoided level crossing. Adiabatic energy levels in full lines, diabatic in dashed lines

time independent Schrödinger equation:

$$H\psi = E\psi \tag{2.2}$$

This gives the eigenvalues:

$$E_{\pm} = \pm\frac{1}{2}\sqrt{4\delta^2 + (vt)^2} \tag{2.3}$$

As we can see, the energy levels will avoid crossing, something we will also refer to as an anti crossing. The properties of the state will however switch at the point when the states are at their closest. Far from the crossing the diabatic and adiabatic basis are the same but close to the crossing they are different. We can see from eq. (2.3) that the closest the levels get is 2δ. If the driving speed is small enough or the coupling is strong enough, the system will stay in the adiabatic state it is initialized to, according to the adiabatic theorem [17]. In the following section we will look at what happens when this is not the case.

2.2 Derivation of the Landau-Zener formula

The details of what happens around the crossing is complicated, so we are not going to try to solve the problem for a general times, but instead try to find what happens when we let the system propagate from $t = -\infty$ to $t = \infty$, by using contour integration. This derivation is based on the derivation done by Curt Wittig [18], with modifications suggested by Le Tuan Anh Ho and Liviu F. Chibotaru [19]. We are going to look at the Hamiltonian, again in the diabatic basis:

$$H = \begin{bmatrix} vt/2 & \delta \\ \delta & -vt/2 \end{bmatrix} \tag{2.4}$$

We look at the evolution from $t = -\infty$ to $t = \infty$. The wave function is going to be on the form:

$$|\psi\rangle = A\,|0\rangle + B\,|1\rangle \tag{2.5}$$

With the time dependent coefficients A and B. We initialize in the lower state so $|A(-\infty)|^2 = 1$. As mentioned we only care about the asymptotic behaviour, we are therefore going use:

$$\int_{-\infty}^{\infty} \frac{\dot{A}}{A} dt = \ln \frac{A(\infty)}{A(-\infty)} \tag{2.6}$$

We know the denominator and we are trying to find the numerator in the logarithm. Assuming that $\frac{\dot{A}}{A}$ is well behaved in the complex plane, we can use Cauchy's integral theorem to get the equation:

$$\int_{-\infty}^{\infty} \frac{\dot{A}}{A} dt = -\int_{C'} \frac{\dot{A}}{A} dz. \tag{2.7}$$

Where C' is the (upper or lower) half circle path in the complex plane centered at $t = 0$, paths being shown in figure 2.2. Because a closed integral in the complex plane over a function with no poles is zero. The quantity we need to find is then $\frac{\dot{A}}{A}$ in the limit of $t \to \pm\infty$ and then we can analytically continue this to the complex plane. If we insert (2.5) into the Shrödinger equation:

$$i\frac{d}{dt}\,|\psi(t)\rangle = H\,|\psi\rangle \tag{2.8}$$

We get the two equations:

$$\dot{A} = -\frac{ivt}{2}A - i\delta B \tag{2.9}$$

$$\dot{B} = -i\delta A + \frac{ivt}{2}B \tag{2.10}$$

Giving us a differential equation for A

$$\ddot{A} + \left(\frac{iv}{2} + \delta^2 + \left(\frac{vt}{2}\right)^2\right) A = 0 \tag{2.11}$$

Next we are going to use some physical knowledge about the system. We know that the transfer *probability* long before and after the transition at $t = 0$ is going to converge to a value, meaning that the modulus of the complex coefficient A is going to converge to a constant value. For large positive or negative times we can thereforee write the amplitude A:

$$A(t) = |A|e^{-i\phi(t)} \tag{2.12}$$

Inserting this into eq. (2.11), we get:

$$\left(-\dot{\phi}^2 - i\ddot{\phi} + \frac{iv}{2} + \delta^2 + \left(\frac{vt}{2}\right)^2\right) |A| = 0 \tag{2.13}$$

Because ϕ is real we can separate this into the real and imaginary parts, we get in the limit of $\pm$ infinite time:

$$\dot{\phi} = \pm\frac{1}{2}\sqrt{4\delta^2 + (vt)^2} \tag{2.14}$$

$$\ddot{\phi} = \frac{v}{2} \tag{2.15}$$

Modifying the first equation we get for $t \to \pm\infty$:

$$\begin{aligned}\dot{\phi} &= \pm\frac{1}{2}v|t|\sqrt{1 + \left(\frac{2\delta}{(vt)}\right)^2} \\ &\approx \pm\left(\frac{1}{2}v|t| + \frac{\delta^2}{v|t|}\right)\end{aligned} \tag{2.16}$$

The two signs corresponds to the two limits $t \to \infty$ and $t \to -\infty$ and so we can remove the $\pm$ and the absolute values

$$\dot{\phi} \approx \left(\frac{1}{2}vt + \frac{\delta^2}{vt}\right) \tag{2.17}$$

We now have what we need to do the contour integral:

$$\frac{\dot{A}(t)}{A(t)}_{t\to\pm\infty} = -i\dot{\phi}_{t\to\pm\infty} \tag{2.18}$$

Because $\frac{\dot{A}(t)}{A(t)}$ has the same limit for $\pm\infty$ and $\frac{\dot{A}(z)}{A(z)}$ is analytic in the integrated domain of the complex plane, we can use analytic continuation and we get the expression for $\frac{\dot{A}(z)}{A(z)}$ we needed:

$$\frac{\dot{A}(z)}{A(z)}_{|z|\to\infty} = -i\left(\frac{1}{2}vz + \frac{\delta^2}{vz}\right) \tag{2.19}$$

The right hand side of (2.7) is then:

$$-\int_{C'}\frac{\dot{A}}{A}dz = i\int_{C'}\left(\frac{1}{2}vz + \frac{\delta^2}{vz}\right)dz \tag{2.20}$$

Introducing the change of variables $z = Re^{-i\theta}$ we get:

$$\begin{aligned}-\int_{C'}\frac{\dot{A}}{A}dz &= i\int_0^{\pm\pi}\left(i\frac{v}{2}R^2e^{2i\theta} + i\frac{\delta^2}{v}\right)d\theta \\ &= \mp\frac{\pi\delta}{v}\end{aligned} \tag{2.21}$$

Where the minus sign in the result of eq. (2.21) correspond to the upper half circle and the plus sign corresponds to the lower, shown in red and blue respectively in figure 2.2.

We can then use eqs. (2.6), (2.7) and (2.21) to get:

$$|A(\infty)|^2 = |A(-\infty)|^2 e^{\mp\frac{2\pi\delta^2}{v}} \tag{2.22}$$

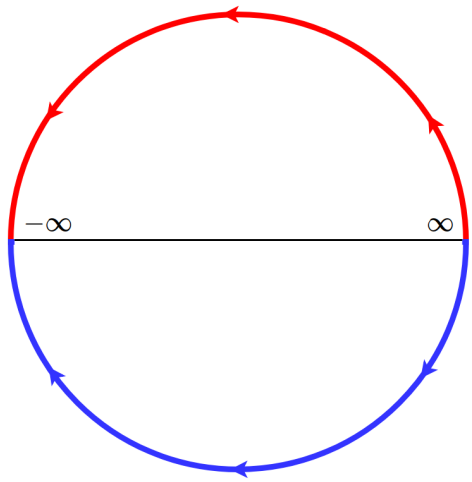

Figure 2.2: Contours along which the complex integrals were taken

The choice of sign can then be made on physical grounds, we are talking about a probability and so we need the negative sign to keep it between 0 and 1, since δ and v are both defined positive. $|A(-\infty)|^2 = 1$ is a initial condition, giving the Landau Zener formula:

$$P_{LZ} = |A(\infty)|^2 = e^{-2\pi\frac{\delta^2}{v}} \tag{2.23}$$

The most common derivation of this formula is one that rewrites the Hamiltonian in a way such that the Shrödinger eq. is on the form of the second-order Weber equation. The solution to this is known and are combinations of parabolic cylinder functions, but finding the asymptotes of this gives the simple equation above [10]. The advantage of this approach is that we can take general limits if needed, though in most cases this is not done and the derivation above is simpler to follow.

2.2.1 Perturbation theory

In order to connect this problem to a more familiar approach we will evaluate the same transition probability using time independent perturbation theory, and show that one obtains the same result as in the derivation above, to first order. If we look at the system with no perturbation, that is just two uncoupled levels. The two levels will pass through each other and the system will stay in the diabatic state. We have defined the LZ probability to be the probability of transfer in the adiabatic basis, and so the zeroth order result is, $P_{LZ}^{(0)} = 1$. Now we can have a look at the first order correction. We look at the same system as in the previous section, a TLS with coupling δ, where we shift one of the levels with vt, v being the sweep speed parameter.

The Hamiltonian of the system is then:

$$H = \begin{bmatrix} 0 & \delta \\ \delta & \Delta(t) \end{bmatrix} \tag{2.24}$$

Where $\Delta(t) = vt + \epsilon(t)$, and $\epsilon(t)$ is Gaussian white noise with the property

$$\langle \epsilon(t)\epsilon(t') \rangle = \gamma\delta(t - t') \tag{2.25}$$

Where γ is some real constant. Adding this noise term is a trick to help us solve an integral later in the derivation, but we will take the limit $\gamma \to 0$ in the final result. The brackets symbolize average over noise.

We introduce transformation:

$$U = \begin{bmatrix} 1 & 0 \\ 0 & e^{-i\phi(t)} \end{bmatrix} \tag{2.26}$$

Where $\phi(t)$ is such that $\dot{\phi} = \Delta(t)$, giving:

$$\phi(t) = \frac{1}{2}vt^2 + \int \epsilon(t')dt \tag{2.27}$$

Applying this transformation to the Schrödinger eq. we get that the transformed Hamiltonain is on the form:

$$\tilde{H} = UHU^\dagger + i\frac{\partial U}{\partial t}U^\dagger \tag{2.28}$$

Which gives us:

$$\tilde{H} = \begin{bmatrix} 0 & \delta e^{-i\phi(t)} \\ \delta e^{i\phi(t)} & 0 \end{bmatrix} \tag{2.29}$$

Now we can turn to time dependent perturbation theory and the interaction picture. $\tilde{H}(t) = H_0 + H'(t)$, where now H_0 now is the diagonal time independent part of Hamiltonian, notice that this is zero because we did the transformation in the beginning, and the off-diagonal time dependent part is $H' = \tilde{H}$. To first order we have:

$$\begin{aligned} |\langle 1| H' |0\rangle|^2 &= \delta^2 \int_{t_0}^{t} dt_1 \int_{t_0}^{t} dt_2 e^{i\phi(t_1)} e^{-i\phi(t_2)} \\ &= \delta^2 \int_{t_0}^{t} dt_1 \int_{t_0}^{t} dt_2 \exp\{i(\frac{1}{2}vt_1 + \int_{t_0}^{t_1} \epsilon(t')dt')\} \\ &\times \exp\{-i(\frac{1}{2}vt_2 + \int_{t_0}^{t_2} \epsilon(t')dt')\} \\ &= \delta^2 \int_{t_0}^{t} dt_1 \int_{t_0}^{t} dt_2 \exp\{i(-\frac{1}{2}v\tau k - \int_{t_1}^{t_2} \epsilon(t')dt')\} \end{aligned} \tag{2.30}$$

Where now $\tau = t_2 - t_1$ and $k = t_1 + t_2$. We move to these variables instead and acquire a factor $-\frac{1}{2}$ because of the Jacobian. We set the boundaries of the integrals to $\pm\infty$, making the boundaries for the new variables the same.

$$|\langle 1| H' |0\rangle|^2 = -\frac{1}{2}\delta^2 \int_{-\infty}^{\infty} dk \int_{-\infty}^{\infty} d\tau \exp\{i(-\frac{1}{2}v\tau k + \int_{t_1}^{t_2} \epsilon(t')dt')\} \tag{2.31}$$

We now make use of the properties of the Gaussian white noise. Averaging the whole expression over all possible noise. What we end up needing to find is:

$$\langle \exp\{i \int_{t_1}^{t_2} \epsilon(t')dt'\}\rangle \tag{2.32}$$

We then use that for Gaussian variables, $\langle e^{if}\rangle = e^{\langle -\frac{1}{2}f^2\rangle}$ and the properties of the noise to find:

$$\langle \exp\{i \int_{t_1}^{t_2} \epsilon(t')dt'\}\rangle = \exp\{-\frac{1}{2}\int_{t_1}^{t_2}\int_{t_1}^{t_2} \langle\epsilon(t')\epsilon(t'')\rangle dt'dt''\} \tag{2.33}$$

$$= \exp\{-\frac{1}{2}\gamma|\tau|\} \tag{2.34}$$

Now we can start to solve the τ-integral:

$$-\frac{1}{2}\delta^2 \int_{-\infty}^{\infty} dk \int_{-\infty}^{\infty} d\tau \exp\{i(-\frac{1}{2}v\tau k) - \frac{1}{2}\gamma|\tau|\} \tag{2.35}$$

$$= -\frac{1}{2}\delta^2 \int_{-\infty}^{\infty} dk \frac{-2i}{-\frac{1}{2}vk + \frac{1}{2}\gamma i} \tag{2.36}$$

$$= -\frac{1}{2}\delta^2 \int_{-\infty}^{\infty} dk \frac{-vki - \gamma}{(-\frac{1}{2}vk)^2 + (\frac{1}{2}\gamma)^2} \tag{2.37}$$

The first term (the imaginary part) is an odd function of k (after a shift of variables) so they drop out. The third term is real and looks like a Lorentzian (Cauchy distribution):

$$L(x) = \frac{1}{2\pi}\frac{\Gamma}{(x-x_0)^2 + (\frac{1}{2}\Gamma)^2}$$

The distribution is normalized to 1, comparing with our integral: $x = -\frac{1}{2}vk$ (giving the factor $\frac{-2}{v}$), $\Gamma = \gamma$ and $x_0 = 0$, also we have a factor 2π. This gives:

$$P_1 = |\langle 1|\, H'\, |0\rangle|^2 = -\frac{2\pi\delta^2}{v} \tag{2.38}$$

Which is the first order result we expect, but as we see the first order result is rather cumbersome to find.

2.3 Multiple Crossings: Landau-Zener-Stückelberg interferometry

The formalism in the this chapter is developed under the assumption that we drive the levels from infinitely far away, through each other and then infinitely far apart again. This assumption is needed to get a simple exact analytic result, but the transition is fairly local. It can be shown that most of the transition happens in a time $t_{LZ} \sim \frac{\sqrt{a}}{\delta}\max(1,\sqrt{a})$ [20]. This means that the effects of the crossings are fairly localized around the time of the crossing, or at least can

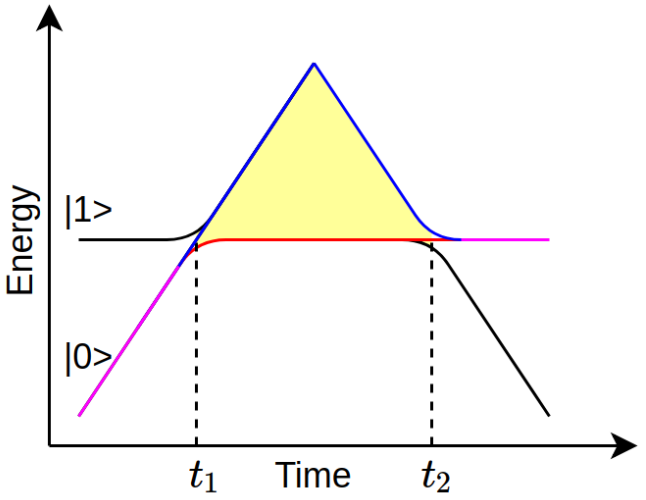

Figure 2.3: Energy spectrum of example described in section 2.3, showing the two paths in red and blue that lead to transfer from the lower driven level. The difference in dynamic phase they acquire corresponds to the yellow shaded area.

be. We can thereforee have successive crossing and still use the same formula for the transfer probability.

Having multiple crossings opens up the possibility of getting interference effects. Say that you initialize the system in the lower of two states, $|0\rangle$, and then drive this level through the other and then back, the energy spectrum is shown in figure 2.3. You can then have two paths that leads to transfer to the stationary level, $|1\rangle$, corresponding to transferring at the first or the second crossing, at times t_1 and t_2 in the figure. The two paths can be seen red and blue in figure 2.3. The paths pick up different dynamical phases along the way, the difference between these phases are known as a Stückelberg phase, and can be seen as the yellow shaded area in figure 2.3. This phase will affect the probability of transfer, which is the idea behind Landau-Zener-Stückelberg interferometry [10]. What phase the system picks up might depend on a physical variable we are interested in measuring, and hence the probability of being in either of the states depends periodically on this variable. We will come back to the concept of Landau-Zener-Stückelberg interferometry in the next chapter, and we will also take inspiration from these interferomtry experiments to design our own in a later chapter.

Chapter 3

Classical driving of few-level systems

In this chapter we are going to introduce a few theoretical approaches to describe classical driving of quantum FLSs. We are going to look at the adiabatic impulse model and the rotating wave approximation. What we mean by classical driving is that we don't take the quantum nature of the driving field into account. The classical driving is introduced as periodic terms in the Hamiltonian describing the FLS. Before doing that, we are going to go over some the numerical methods we will be using in this and following chapters, giving us something to compare our analytical results with.

3.1 Simulations

All simulations in this thesis is going to be done Python with a library called QuTip [21, 22]. This package introduces quantum objects in Python, like the function `basis()` that makes a basis ket, or the function `coherent_dm()` which makes a coherent state density matrix in the desired dimension and expectation value. It also has a set of master equation solvers that will enable us to propagate quantum states in time, given a Hamiltonian. The way this is done is by constructing the time independent part of the Hamiltonian on matrix form (`H0`), using the quantum objects we mentioned, then constructing the time dependent parts of the Hamiltonian split into a constant matrix (`H1`) and a time dependent coefficient in the form of a function (`H1_coeff`). The whole Hamiltonian is then assembled in a list, an example of such a list being, `H = [H0,[H1,H1_coeff]]`. This list is then fed into the solver function, the one used in this thesis is named the Lindblad Master Equation Solver (named `mesolve()` in QuTip). The Lindblad master equation is describing evolution of a density matrix that follows the laws we are used to in quantum mechanics. The LMES also takes a initial state, a list of times and optionally a list of operators. The function returns the evolved state and the expectation values of the operators given at the times listed. The states and expectation values returned can then be manipulated, modified and/or visualized (the library contains a wide array of visualisation functions, like plotting the Wigner distribution or the Fock distribution). The library also contains different master equation solvers and a function using Monte Carlo simulation, but they are used in the same manner and have similar run times within the scope of this thesis.

Examples of code can be found in appendix B.

3.2 Periodic driving

The example we are going to look at is what happens when we introduce periodic driving in FLSs. In the case of the TLS, we will have Hamiltonians in the diabatic basis:

$$H_l = (A\cos\omega t + \Delta)/2\sigma_z + \delta\sigma_x \tag{3.1}$$

$$H_t = \Delta/2\sigma_z + (A\cos\omega t + \delta)\sigma_x \tag{3.2}$$

The first Hamiltonian, H_l, describes what we call longitudnial driving, we call it that because of the σ_z in the driving term, and is as we can see driving of the energy levels. The second Hamiltonian, H_t, describes what we call transverse driving, this time the name referrs to the σ_x matrix.

3.2.1 Rotating wave approximation

What we are going to look at in this section is a well known problem called the Rabi problem. It is that of a two level atom in a harmonic field, with a frequency close to the natural frequency of the atom. What we will see is that the system will oscillate between the two states of the system. This is commonly referred to as Rabi oscillations or Rabi flopping. We will focus on the longitudinal driving in this problem, and we define the $|0\rangle$ state to have zero energy:

$$H_l = -(A\cos\omega t + \Delta)\,|1\rangle\langle 1| + \delta(|0\rangle\langle 1| + |0\rangle\langle 1|) \tag{3.3}$$

We are first going to find a transformation that move the oscillating term off the diagonal, making the problem of transverse and longitudinal driving pretty much the same. To find such a transformation, we take a look at what transformation does to the Hamiltonian, by applying the general unitary transformation to the Schrödinger eq.

$$\begin{aligned} Ui\frac{\partial}{\partial t}|\psi\rangle &= UH|\psi\rangle \\ &= UHU^\dagger U|\psi\rangle \end{aligned} \tag{3.4}$$

Using the chain rule in reverse on the left hand side, we get:

$$i\frac{\partial}{\partial t}(U|\psi\rangle) = \left(UHU^\dagger + i\frac{\partial U}{\partial t}U^\dagger\right)U|\psi\rangle \tag{3.5}$$

Giving the effective Hamiltonian for the transformed state, $U|\psi\rangle = |\tilde{\psi}\rangle$. After the transformation:

$$\tilde{H} = UHU^\dagger + i\frac{\partial U}{\partial t}U^\dagger \tag{3.6}$$

We notice that transformations on the form $e^{-i\eta}$, where η is a diagonal matrix, will leave the diagonal invariant under the $UHU^\dagger$ term, and will add the matrix $\frac{\partial\eta}{\partial t}$, because of the derivative term in the effective Hamiltonian. So to have the desired effect we set:

$$\eta = -|1\rangle\langle 1|\int A\cos(\omega t)dt = -|1\rangle\langle 1|\frac{A}{\omega}\sin(\omega t) \tag{3.7}$$

As we can see the transformation only affects the relative phases of the two coefficients in the wave function. So now our transformed Hamiltionan looks like:

$$\tilde{H}_l = \delta(e^{-i\frac{A}{\omega}\sin(\omega t)} \left|1\right\rangle \left\langle 0\right| + h.c.) + \Delta \left|1\right\rangle \left\langle 1\right| \tag{3.8}$$

Luckily there is an identity that simplifies this quite a bit.

$$e^{i\chi \sin\tau} = \sum_{n=-\infty}^{\infty} J_n(\chi) e^{in\tau} \tag{3.9}$$

Which leaves us with the transformed longitudinal Hamiltonian:

$$\tilde{H}_l = (\sum_{n=-\infty}^{\infty} \delta J_n(\frac{A}{\omega}) e^{-in\omega t} \left|1\right\rangle \left\langle 0\right| + h.c.) - \Delta \left|1\right\rangle \left\langle 1\right| \tag{3.10}$$

While the transverse Hamiltonian on the same form looks like:

$$\begin{aligned} H_t &= (A\cos(\omega t) \left|1\right\rangle \left\langle 0\right| + h.c.) - \Delta \left|1\right\rangle \left\langle 1\right| \\ &= (A\frac{e^{-i\omega t} + e^{i\omega t}}{2} \left|1\right\rangle \left\langle 0\right| + h.c.) - \Delta \left|1\right\rangle \left\langle 1\right| \end{aligned} \tag{3.11}$$

We can now see how similar the two Hamiltonians, H_l and H_t, really are. both having harmonic terms on the off-diagonal. The procedure forward is similar for the two Hamiltonians, but we continue to focus on the longitudinal Hamiltonian. We introduce a transformation to a rotating frame:

$$V = \exp\left(-ik\omega t \left|1\right\rangle \left\langle 1\right|\right) \tag{3.12}$$

Giving us the transformed Hamiltonian:

$$\tilde{H_l}' = (\sum_{n=-\infty}^{\infty} \delta J_n(\frac{A}{\omega}) e^{-in\omega t} e^{ik\omega t} \left|1\right\rangle \left\langle 0\right| + h.c.) + (-\Delta + k\omega) \left|1\right\rangle \left\langle 1\right| \tag{3.13}$$

We are going to look at the case of single photon transfer so we set $k = 1$. We now get to the approximation, assuming that $\Delta, \omega \gg \delta J_k(\frac{A}{\omega})$ and that $\Delta - \omega$ is small, we can neglect everything that is still oscillating. This is what is known as the rotating wave approximation. What it does is that picks out the harmonic terms with a frequency equal to the natural frequency of the system. Giving us the final time independent Hamiltonian:

$$H_{RWA} = (-\Delta + \omega) \left|1\right\rangle \left\langle 1\right| + (\delta J_1(\frac{A}{\omega}))\sigma_x \tag{3.14}$$

Which can then be solved as a fairly simple eigen-value/function problem, if we then find the probability of the system being in the $|0\rangle$ state we end up with what is called the Rabi formula:

$$P(t) = |\left\langle 0|\psi(t)\right\rangle|^2 = \frac{|\delta'|^2}{\frac{1}{4}\Delta^2 + |\delta'|^2} \sin^2\left(\sqrt{\frac{1}{4}\Delta^2 + |\delta'|^2}t\right) \tag{3.15}$$

Where $\delta' = \delta J_1(\frac{A}{\omega})$. What is referred to as the Rabi frequency is then $\Omega_r = \sqrt{\frac{1}{4}\Delta^2 + |\delta'|^2}$

3.2.2 Strong longitudinal driving: Landau Zener Stückelberg interferometry

We will here be working in the adiabatic basis, looking at the same problem as above, but this time we look at large amplitudes, so large that the levels cross. We also assume that the coupling between the levels is small compared to the maximum level splitting. In reality the evolution smoothly goes between regions where it evolves almost adiabatically and regions that are non-adiabatic, but assuming that the system linearly transverses the crossing region, we can assume instantaneous transitions with adiabatic evolution elsewhere and still get an accurate description of the evolution of the system [10]. This is known as the adiabatic impulse model and is a tool for working with these kinds of systems. The level crossings can be modeled as LZT, since they are roughly linear in the case of harmonic driving with a large amplitude compared to the level splitting.

We can then make a fairly intuitive picture of what is going on. If we initialize the system in the lower level, and want to know the probability of it ending up in the upper level, we have to consider all the different paths it can take to get there. It can transfer at the first level crossing or the second and so on. We have to take into account that these paths can interfere, example of two such paths in figure 3.1, in red and blue. How these paths interfere depend on the phase acquired between when they separate and when they recombine. The difference in dynamical phase between the two paths can be seen as the area between the paths in an energy time diagram, this phase is referred to as a Stückelberg phase. In the case of paths in figure 3.1 this phase difference would be $2K - L$.Then there is also a so-called geometric phase picked up along each path, associated with the detailed dynamics close to the level crossings; we will come back to this. To find the full probability of transfer, we then need to sum up all such paths. If the frequency of the driving is just right (that is, the frequency is the corresponding to the level splitting), we will get oscillations in the occupation between the levels. As shown in [10] we indeed get the same result as we found when we looked at the problem with the RWA approach.

Keeping track of all the paths and transfer probabilities of all the crossings can be hard, and we therefore look at a formalism where an evolution operator for the whole process is made. This evolution operator is going to be made up of adiabatic evolution operators with operators in between representing the non adiabatic crossing that changes the population of the levels and add these geometric phases.

$$U_{total}(t_i, t_f) = U(t_n, t_f) \dots NU(t_1, t_2)NU(t_i, t_1) \tag{3.16}$$

These operators are in the adiabatic basis, $\{|E_+\rangle, |E_-\rangle\}$ given by:

$$N = \begin{bmatrix} \sqrt{1 - P_{LZ}}e^{-i\phi_s} & -\sqrt{P_{LZ}} \\ \sqrt{P_{LZ}} & \sqrt{1 - P_{LZ}}e^{i\phi_s} \end{bmatrix} \tag{3.17}$$

$$U(t, t') = \begin{bmatrix} e^{-i\int_t^{t'} E_+ dt} & 0 \\ 0 & e^{-i\int_t^{t'} E_- dt} \end{bmatrix} \tag{3.18}$$

The phases in eq. (3.18) are the dynamically acquired phases we get from solving the Schödinger equation. And $E_\pm$ are the instantanous energy eigenvalues of the adiabatic states $|E_\pm\rangle$, found by solving the time independent Schrödinger equation

$$H|E_\pm\rangle = E_\pm |E_\pm\rangle \tag{3.19}$$

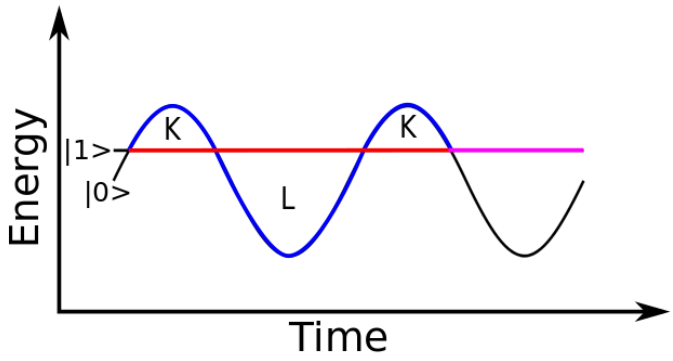

Figure 3.1: Example of two paths that will interfere when they recombine, how they interfere depends on the areas K and L

P_{LZ} is acquired form the LZ formula.

$$P_{LZ} = e^{-2\pi \frac{\delta^2}{v}} \tag{3.20}$$

Where $\langle 0| H |1\rangle = \delta$ and v is the driving speed at the crossing. In our derivation of the LZ formula we only cared about the probability of transfer. What this neglects are some phases that are acquired during a crossings. There is a geometric phase that we get when transferring in the diabatic basis, ϕ_S. This phase can be found using the other derivation of the LZ probability we mentioned in section 2.2, shown in [10]. This phase can be expressed by the adiabacity parameter $a = \delta^2/v$ as:

$$\phi_s = \phi_s' - \frac{\pi}{2}\phi_s' = \frac{\pi}{4} + a(\ln a - 1) + \arg\Gamma(1 - ia) \tag{3.21}$$

Where ϕ_s' is the so-called Stokes phase. In the case of periodic driving, simplifications can be made, since every other adiabatic evolution operator are the same. We can bunch them together and write the total for an even number of crossings as:

$$U_{total} = U(t_n, t_f)\left(NU(t_1, t_2)NU(t_i, t_1)\right)^m \tag{3.22}$$

The term in the parentheses can then be diagonalized and then taking the power is simple. The same can then be done for an odd number of transitions, and for a more use full result the time average can be taken. This approach gives the same results as the RWA, giving the Rabi formula, as is shown in [10].

Chapter 4

Application: Classically driven nitrogen-vacancy center as a magnetometer

We now have a small set of methods that can be useful in many different applications. We take a closer look at one such application. We will investigate the use of a single negatively charged nitrogen-vacancy center in diamonds (hereby referred to as a NV center) as a magnetometer. This is a crystal point defect that consist of a vacancy and a nitrogen atom in diamonds. Associated with this defect are two electrons, which can as we know make triplet states or a singlet state. The energy of the ground state singlet state is currently not known, but it is generally accepted that the singlet state has a higher energy than the triplet states [23], meaning that the three lowest states of the system are the three triplet states. In these three states the pair of electrons have a total spin projection of, $s_z = 0, +1$ and -1. The system can be described by the Hamiltonian, as [24]:

$$H = hDS_z^2 + hE\left(S_x^2 - S_y^2\right) + g\mu_B \boldsymbol{B} \cdot \boldsymbol{S} \tag{4.1}$$

Due to strain in the crystal there will be a zero field splitting between the energy eigenvalues of the $|0\rangle$ state, the state with $s_z = 0$ and the two parallel spin states $|+1\rangle$ and $|-1\rangle$, the states with $s_z = \pm 1$. In the Hamiltonian above, the magnitude of this is given by the zero field splitting parameter D, this parameter is temperature dependent, which can be problem for magnetic measurements using this system. The zero field splitting parameter E also comes from local strain in the crystal, affecting the symmetry of the system and effectively mixing the two states $|\pm 1\rangle$, but this is in general small compared to the other zero field splitting. Typical values of these two parameters in a nanodiamonds are $D \approx 2.87GHz$ and $E = 5MHz$. The parameter E is very dependent on the type of diamond, e.g. it is much smaller in high purity chemical vapour deposition grown diamond samples, where it can be as low as $E \approx 100KHz$ [24].

The two states $|\pm 1\rangle$ have opposing spin meaning that the difference in energy between them is affected by the presence of a magnetic field, described by the last term in the Hamiltonian,

this is known as the Zeeman effect [5]. That means that if we know the level splitting, we also know the magnetic field. The electron spins associated with NV-centers generally have very long coherence times, this is due to the defect being isolated from spin noise by the carbon-12 environment. Naturally sourced carbon samples will be dominantly spin-less carbon-12, meaning that even without doing anything to the carbon we have a good environment to put a quantum system. It can be made even better by enriching the sample so that it is close to pure carbon-12, making the coherence dephasing times very long (in the order of ms) even at room temperature [25]. This is one of the strongest selling points of NV-centers as magnetometers. Most quantum devices needs to be cooled to close absolute zero for them to be useful, which makes them expensive, large and cumbersome to use. The NV-center however is very well isolated and insensitive to disturbances.

The idea of a NV-center magnetometer has been investigated a lot in the last decade both using mainly just the two upper levels [26, 27, 28, 29] and using the full spin-1 nature of the system [6]. In this second paper a method using the whole spin-1 nature of the system is investigated, after initializing i the $|0\rangle$ state they use that a microwave field only drives transition from $|0\rangle$ to a certain superposition of the $|\pm 1\rangle$ states, what they call a bright state. They then let this superposition evolve, and how fast it oscillates between this bright state and the orthogonal state, the dark state, depends on the level splitting between $|-1\rangle$ and $|+1\rangle$. When a microwave field is turned on again, the bright state transfers back to the $|0\rangle$ state. This method is fairly insensitive to temperature fluctuations. How much of the state that returns can be measured and is then a periodic function of the levels splitting.

The initialization and readout in the method above is done via something referred to as pumping, this is done by shining a specific frequency of light on the NV-center. Having a look at figure 4.1, which shows a schematic of the energy spectrum for some of the lower states of the system, we see that the system has exited triplet states as well as two intermediate singlet states on with higher energy than the triplet states. The excited $s_z = 0$ state of the triplet, $|0\rangle_e$, is mainly going to decay via radiation, represented by the red arrow. This means that if the system is excited in this way, it will relax to the $|0\rangle_g$. While the exited states $|\pm 1\rangle_e$ have non radiative paths back toground state triplet, represented by the black dotted arrows in figure 4.1, as well as radiative paths represented by red arrows. Doing this many times we can be as sure as we want that the system is in $|0\rangle_g$, since once it is there, more pumping will keep it there. For the measurement it is the same idea, since the exited $s_z = \pm 1$ triplet states have non radiative paths back to the ground state triplet, excitation and then fluorescence is a sign that the system is in $|0\rangle_g$. If the system is in the $|\pm 1\rangle$ states there is a chance of it being exited and then decaying without fluorescing and so the intensity of light goes down. The emitted light will be at a lower frequency, this is something called a Stokes shift. So the pumping is done by a green laser, while the NV-center fluoresces with red light. These processes are described in [23].

4.1 Trapezoid level sweeping

One approach to measuring magnetic fields with a NV-center is to take inspiration from Landau-Zener-Stückelberg interferometery. Let us assume for now that we have full control over the energy of the lowest level, which in reality might not be feasible, but we will come back to this. We drive the lower level through both of the upper levels, wait for some time and drive it back through the levels, as is shown in figure 4.2. Talking in the language of paths that we

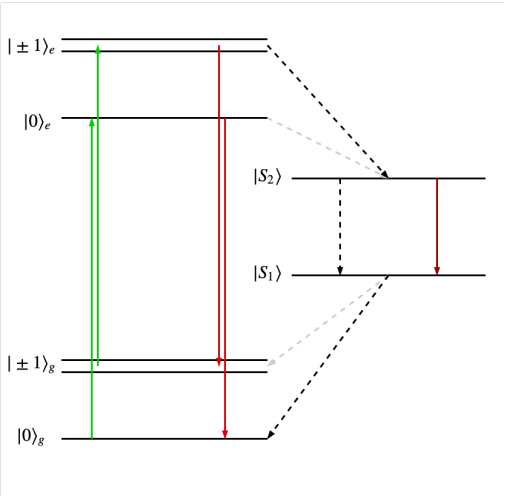

Figure 4.1: The level structure of NV-centers in diamond, only qualitativly. With transitions, the coloured arrows are radiative transitions and are the main contribution. The colour is roughly representing the colour of the light. The black and grey dotted arrows represent the non radiative decays. The light gray transitions are less likely.

mentioned when talking about LZS interferometery, there are then three paths the system can take that leads back to the $|0\rangle$ state, marked in colors in figure 4.3. On each path it will acquire different a phase, and the difference between these should carry information about the level splitting between the two upper levels Δ, shown in figure 4.2. In particular the phase difference between the two lower paths, again shown in blue and red in figure 4.3, is clearly dependent on the level splitting. In the diabatic basis the Hamiltonan of the system is:

$$H = \begin{bmatrix} \Delta/2 & 0 & \delta \\ 0 & -\Delta/2 & \delta \\ \delta & \delta & \epsilon(t) \end{bmatrix} \tag{4.2}$$

The driving term $\epsilon(t)$:

$$\epsilon(t) = \begin{cases} vt - D & t < (D+\zeta)/v \\ \zeta & (D+\zeta)/v < t < (D+\zeta)/v + \tau \\ -v(t - (D+\zeta)/v - \tau) + \zeta & t > (D+\zeta)/v + \tau \end{cases} \tag{4.3}$$

Where v is the slope of the driving, ζ is how far above the middle of the two upper level the lower level is driven, D is again the zero field splitting between the lower level and the two upper levels and τ is the time where the system is stationary. Again a visualisation of the energy levels can be seen in 4.2.

To analyse this problem we are going to use the adiabatic impulse model, i.e. adiabatic evolution everywhere except at the level crossings. Another approximation we are going to make is saying that the adiabatic crossing regions are going to be small. So when calculating the phase acquired, we are going to use the diabatic energy levels, as the phases we get from these are much simpler.

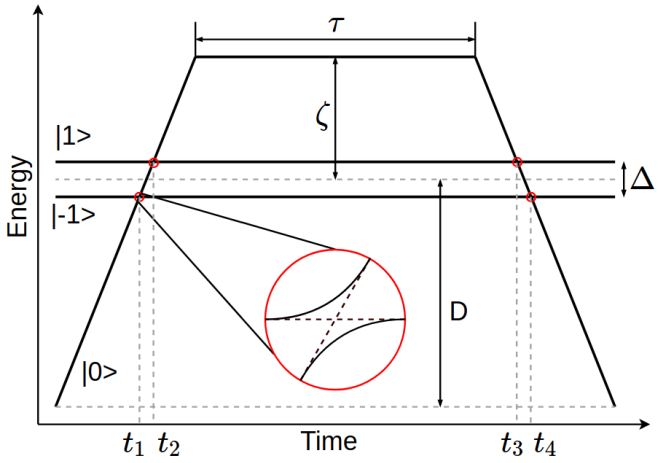

Figure 4.2: Illustration of the procedure to measure magnetic field. Red rings at avoided level crossing and inset showing the diabatic (dotted) and adiabatic (full line) levels

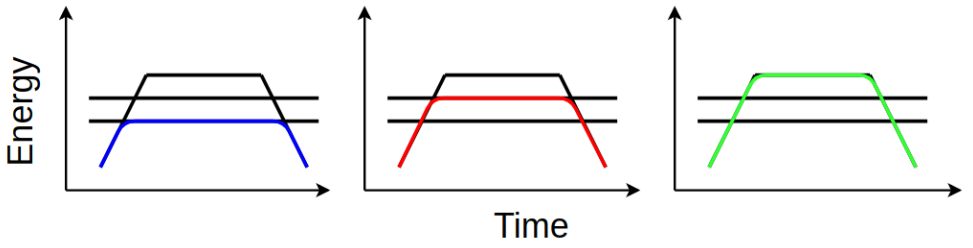

Figure 4.3: The three paths the system can take, initialized in the lower of the three states

4.1.1 Non-adiabatic evoultion

The Landau Zener transfer matrix in eq. (3.17) is defined for a two level system. We generalize for the two transitions in the case of the ThLS where the two bottom levels cross, using the same convention as in section 3.2.2 working with the basis of instantaneous eigenstates in order of increasing energy:

$$N_1 = \begin{bmatrix} 1 & 0 & 0 \\ 0 & \multicolumn{2}{c}{\multirow{2}{*}{$\mathbf{N}$}} \\ 0 & & \end{bmatrix} \tag{4.4}$$

And for the case of the two upper levels crossing

$$N_2 = \begin{bmatrix} \multicolumn{2}{c}{\multirow{2}{*}{$\mathbf{N}$}} & 0 \\ & & 0 \\ 0 & 0 & 1 \end{bmatrix} \tag{4.5}$$

Where the N matrix is defined as in eq. (3.17):

$$N = \begin{bmatrix} \sqrt{1-P_{LZ}}e^{-i\phi_s} & -\sqrt{P_{LZ}} \\ \sqrt{P_{LZ}} & \sqrt{1-P_{LZ}}e^{i\phi_s} \end{bmatrix} \tag{4.6}$$

4.1.2 Adiabatic evolution

As an approximation in the weak coupling limit we can make up the adiabatic energy levels of segments of the diabatic basis. E.g. the lowest adiabatic level, shown in blue in figure 4.3, can approximated by whatever diabatic level has the lowest energy, what level this is change at the first and the last level crossing in this case. We then get adiabatic evolution matrices of the type:

$$U(t_i, t_j) = \begin{bmatrix} e^{-i\phi_1} & 0 & 0 \\ 0 & e^{-i\phi_2} & 0 \\ 0 & 0 & e^{-i\phi_3} \end{bmatrix} \tag{4.7}$$

Where the phases are defined by the energy of the diabatic states, $|1\rangle$, $|-1\rangle$ and $|0\rangle$, E_1, E_{-1} and E_0:

$$\begin{aligned} \phi_1(t_i, t_j) &= \int_{t_i}^{t_j} E_1 dt \\ \phi_2(t_i, t_j) &= \int_{t_i}^{t_j} E_{-1} dt \\ \phi_3(t_i, t_j) &= \int_{t_i}^{t_j} E_0 dt \end{aligned} \tag{4.8}$$

4.1.3 The full evolution and return probability

There is five regions we need to find the adiabatic evolution of. Those are between the two first crossings, after the second crossing and before the system becomes static, the region where the system is static, after the static part before the third crossing and then between the last crossings.

Taking the non adiabatic evolutionary matrices into account as well, we get the full evolution matrix:

$$U(t_i, t_f) = N_1 U(t_4, t_3) N_2 U(\tau_1, t_3) U(\tau_0, \tau_1) U(t_2, \tau_0) N_2 U(t_1, t_2) N_1 \tag{4.9}$$

Where the initial and the final time is respectively t_i and t_f, and the n-th avoided level crossings happen at t_n. We have not included the adiabatic evolution before and after the crossings as this will only give a shifted phase in the end, and we are going to look at the probabilities. The two last adiabatic evolution matrices are the same as the two first so we can simplify to:

$$U(t_i, t_f) = N_1 U(t_1, t_2) N_2 U(t_2, \tau_0) U(\tau_0, \tau_1) U(t_2, \tau_0) N_2 U(t_1, t_2) N_1 \tag{4.10}$$

Where now in the adiabatic basis, the propagation between the first level crossings with the phases defined in section 4.1.2:

$$U(t_1, t_2) = \begin{bmatrix} e^{-i\phi_1(t_1,t_2)} & 0 & 0 \\ 0 & e^{-i\phi_3(t_1,t_2)} & 0 \\ 0 & 0 & e^{-i\phi_2(t_1,t_2)} \end{bmatrix} \tag{4.11}$$

The propagation between the second level crossing and the static phase:

$$U(t_2, \tau_0) = \begin{bmatrix} e^{-i\phi_3(t_2,\tau_0)} & 0 & 0 \\ 0 & e^{-i\phi_1(t_2,\tau_0)} & 0 \\ 0 & 0 & e^{-i\phi_2(t_2,\tau_0)} \end{bmatrix} \tag{4.12}$$

The propagation for the static portion of the sweep:

$$U(\tau_0, \tau_1) = \begin{bmatrix} e^{-i\phi_3(\tau_0,\tau_1)} & 0 & 0 \\ 0 & e^{-i\phi_1(\tau_0,\tau_1)} & 0 \\ 0 & 0 & e^{-i\phi_2(\tau_0,\tau_1)} \end{bmatrix} = \begin{bmatrix} e^{-i\zeta\tau} & 0 & 0 \\ 0 & e^{-i\Delta\tau/2} & 0 \\ 0 & 0 & e^{i\Delta\tau/2} \end{bmatrix} \tag{4.13}$$

To find the evolution of a system initialized in the lower state we apply the evolution matrix we found to it:

$$|\psi_f\rangle = U(t_i, t_f) |\psi_i\rangle = U(t_i, t_f) |\psi_3\rangle = \begin{bmatrix} u_{11} & u_{12} & u_{13} \\ u_{21} & u_{22} & u_{23} \\ u_{31} & u_{32} & u_{33} \end{bmatrix} \begin{bmatrix} 0 \\ 0 \\ 1 \end{bmatrix} = \begin{bmatrix} u_{13} \\ u_{23} \\ u_{33} \end{bmatrix} \tag{4.14}$$

Return probability

We find the return probability by first projecting the state we have now found to the lower state, $|\psi_3\rangle$, and then absolute squaring it:

$$P = |\langle \psi_3 | \psi_f \rangle|^2 = |u_{33}|^2 \tag{4.15}$$

If we set $t_i = t_1 = 0$, the amplitude of the return is going to be:

$$\begin{aligned} u_{33} = & -P_{LZ}^2 e^{-2i(\phi_3(0,\tau_0)+\zeta\tau/2)} \\ & + P_{LZ}(1-P_{LZ}) e^{-2i(\phi_3(0,t_2)+\phi_1(t_2,\tau_0)+\Delta\tau/4-\phi_s)} \\ & + (1-P_{LZ}) e^{-2i(\phi_2(0,\tau_0)+\Delta\tau/4-\phi_s)} \end{aligned} \tag{4.16}$$

From this amplitude we can see what was meant when we said the total propagation is going to be a sum of the paths the system can take. As an example, the first term corresponds to the system taking the path where it transfers at every avoided level crossing (meaning that it doesn't follow the adiabatic energy levels) and ends up back where it started. We see this from the coefficient and from the phase that is acquired. For each path there is an acquired phase from the adiabatic propagation and also this so called Stokes phase. The phases in the equation above could then have been found more directly by finding the areas in the energy-time diagram. Given in terms of the system variables such as swipe speed and swipe amplitude they are:

$$\phi_3(0,\tau_0) = (\frac{\zeta^2 - (\Delta/2)^2}{2v}) \tag{4.17}$$

$$\phi_3(0,t_2) + \phi_1(t_2,\tau_0) = 0 + \left(\frac{\zeta - \Delta/2}{v}\right)(\Delta/2) \tag{4.18}$$

$$\phi_2(0,\tau_0) = \frac{\Delta/2 + \zeta}{2v}\Delta \tag{4.19}$$

We can now find the return probability by taking the absolute square of the amplitude:

$$\begin{aligned} P = {} & P_{LZ}^4 + P_{LZ}^2(1-P_{LZ})^2 + (1-P_{LZ})^2 \\ & - 2P_{LZ}^3(1-P_{LZ})\cos\left(\frac{\Delta^2}{4v} - \Delta(\frac{1}{2}\tau + \frac{\zeta}{v}) + \frac{\zeta}{v}(v\tau+\zeta) + 2\phi_s\right) \\ & - 2P_{LZ}^2(1-P_{LZ})\cos\left(\frac{\Delta^2}{4v} + \Delta(\frac{1}{2}\tau + \frac{\zeta}{v}) + \frac{\zeta}{v}(v\tau+\zeta) + 2\phi_s\right) \\ & + 2P_{LZ}(1-P_{LZ})^2\cos\left(\Delta(\tau + \frac{2\zeta}{v})\right) \end{aligned} \tag{4.20}$$

Where now each of the three last terms corresponds to interference between two paths. E.x. the last term corresponding to the paths where the system propagates via the two upper levels, again in the red and blue paths in figure 4.3.

As we can see in figure 4.4 and comparing the color plots of figure 4.8b and figure 4.5, the analytic result is very similar to the return probability under direct driving. At least in the limit where our approximation of the dynamic phase is valid. In the case where this approximation is not so good, that is in the adiabatic case, the phase is slightly off, but the analytic result and the simulation has the same periodic nature. This could be mended by finding the exact dynamic phases, integrating the adiabatic energy levels.

4.1.4 Measurement

We see that the trapezoid driving of levels can be used to find the magnetic field. One way to do so would be to measuring the return probability for different wait times τ and then take the Fourier transform, which then gives peaks at frequencies corresponding to the splitting between the levels in the stationary part of the driving, Δ, $\zeta - \Delta/2$ and $\zeta + \Delta/2$. This would however be time consuming, and so known methods are probably better. In this section we are going to discuss how we could use the trapezoid system discussed, to measure small changes in the magnetic field. We saw that the return probability has a periodic structure, so what we can do is to find a region of the return probability where it is a one to one map from return probabilities

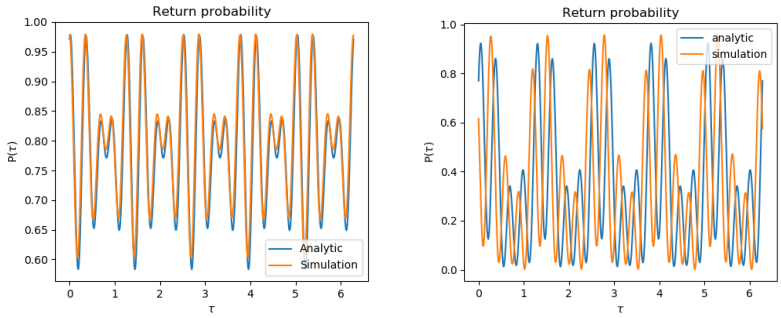

Figure 4.4: Comparing the analytic result we got above, with numerical simulation. To the left the adiabacity parameter is kept low ($P_{LZ} \approx 0.95$), while on the left it is larger ($P_{LZ} \approx 0.5$). Paramaters $\epsilon = 25$, v= 1, $\Delta = 5$, ζ = 15, with $\delta = 0.1$ in the left, and it is the same in the right with the exception of $\delta = 0.3$

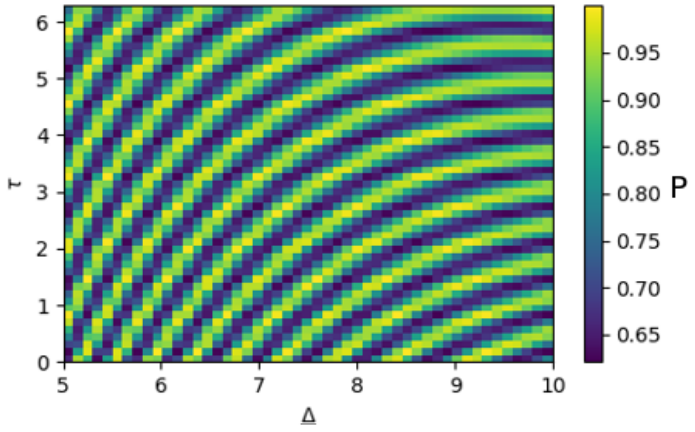

Figure 4.5: Color plot of the analytic results we found in eq. (4.20). With paramaters: $\epsilon = 15$, $\delta = 0.5$, v = 0.7, $\xi = 10$, ξ is how far above the upper of the two stationary levels the sweep goes.

to level splitting. A general approach is to to look at the return probability as a function of level splitting, $P(\Delta)$, and then find the extreme points of this function. The region between two such points would then be the range of level splittings we can measure.

We can then make a list of these extreme points, by derivation, numerical or experimental methods. Then taking the midpoint between any two adjacent extreme points, and use a measure of how good each of these midpoints are to choose which one of these points we want to use. One such measure is signal strength. For a small change in level splitting, $\delta\Delta$, we expect a change in return probability: $\delta P = S = \left|\frac{dP}{d\Delta}\right| \delta\Delta$. So for the best resolution we want $\frac{dP}{d\Delta}$ to be as big as possible, we can also simply use the mean slope between two extreme points or if all we want is contrast, the value of $P(\Delta_2) - P(\Delta_1)$, where the two arguments are extreme points of the return probability. Taking noise into account, signal to noise ratio would be a good measure, since contrast or signal strength also might coincide with sensitivity to noise. We expect a large contributor to the noise to be related to the temperature dependence of D, the zero field splitting between the level having $s_z = 0$ and the ones having $s_z = \pm 1$. The noise due to this is given by

$$N = \left|\frac{dP}{dT}\right| \delta T = \left|\frac{dP}{dD}\right| \frac{dD}{dT} \delta T = \left|\frac{dP}{d\zeta}\frac{d\zeta}{dD}\right| \frac{dD}{dT} \delta T = \left|\frac{dP}{d\zeta}\right| \frac{dD}{dT} \delta T \tag{4.21}$$

Where $\frac{dD}{dT}$ is a known parameter in NV-centers, $\frac{dD}{dT} \approx 75kHz/K$. Signal to noise ratio is then given by:

$$S/N = \frac{\left|\frac{\partial P}{\partial \Delta}\right| \delta\Delta}{\left|\frac{dP}{d\zeta}\right| \frac{dD}{dT} \delta T} \tag{4.22}$$

Looking at where $S/N = 1$ gives us the smallest level splitting we measure and be sure isn't due to noise.

$$\delta\Delta = \frac{\left|\frac{dP}{d\zeta}\right| \frac{dD}{dT}}{\left|\frac{dP}{d\Delta}\right|} \delta T \tag{4.23}$$

4.1.5 Photon-assisted Landau-Zener transitions

The zero field splitting D, that is the splitting between the $|0\rangle$ state and the $|\pm\rangle$ state, is dependent on the stress caused by the pressure P_s. We could therefore think that the driving we have described could be made possible by straining the crystal. However typical numbers for the pressure dependence on the parameter D at room temperature, which has a value of $\approx 2.87GHz$ when no pressure is applied, is $\frac{dD}{d\P_s} \approx 15KHz/MPa$ [30]. Meaning that a pressure $\approx 191GPa$ would be needed to shift the energy by the level splitting. Pressures this high are possible to produce, modulating it on the timescale we are looking at is however clearly impossible.

We do however have the possibility to drive the splitting D with small amplitudes. We saw the emergence of effective energy level when applying the RWA to a periodically driven system. We will call this new level a sideband. This effective energy level was shifted by the frequency of the driving field, and as we will see later this correspond to energy of the bias point of the oscillation and a photon. Notice also that the placement of this level can be tuned with the frequency of the driving. The coupling between this new energy level and the other atom level

is different, but otherwise the problem looks similar to the case of the non driven TLSs. In this section we will therefore investigate LZT between one level and the sideband of another level, what we will call a photon-assisted Landau-Zener transition. The system we are looking at can be represented by the Hamiltonian:

$$H = \begin{bmatrix} 0 & \delta \\ \delta & -\epsilon(t) \end{bmatrix} \tag{4.24}$$

$$\epsilon(t) = \Delta + A\cos(\omega(t)t) \tag{4.25}$$

$$\omega(t) = \omega_0 + \alpha t \tag{4.26}$$

We assume that the frequency is varying slowly, $\alpha \ll \omega_0$, so that we can find the instantaneous solutions and then introduce the time dependence of the frequency later. We then know how to simplify the Hamiltonian with the RWA. Giving us the same Hamiltonian as in section 3.2.1:

$$H_{RWA} = \begin{bmatrix} 0 & \delta J_1(\frac{A}{\omega}) \\ \delta J_1(\frac{A}{\omega}) & -\Delta + \omega \end{bmatrix} \tag{4.27}$$

We can then reintroduce the time dependence of the frequency, so that we have control over the energy of the $|1\rangle$ state. Now we have a fairly simple problem of a stationary level and a linearly moving level, with a avoided level crossing where the gap is $2\delta J_1(A/\Delta) = 2\delta_1$ since the crossing is at $\omega = \Delta$. The LZ-formula gives us the transition probability. The probability of staying in the diabatic sideband that is moving, P_{LZ} is then given by:

$$P = P_{LZ} = \exp(-2\pi a) \tag{4.28}$$

$$a = \frac{\delta_1^2}{\alpha} = \frac{[\delta J_1(\frac{A}{\Delta})]^2}{\alpha} \tag{4.29}$$

This is however not what we see when we do a numerical simulation of such a sideband/level LZT, as we can see figure 4.6. The LZ formula we found gives the wrong transfer probability. A clue to what is happening is that it looks like the system gets to the transition twice as fast as it should; the system starts at $\omega(t) = \omega_0 = 35$, and so we expect the crossing to happen 150 time units later, because the driving speed $\alpha = 0.1$ gives $\omega(150) = \Delta$. But as we see from figure 4.6 the crossing happens after about 75 time units. To see why, we look closer at the time dependence of the oscillating level $\propto \cos((\omega_0 + \alpha t)t) = \cos(f(t))$. The change in frequency is slow compared to the frequency, so lets look at how the time dependence is locally in time. We Taylor expand the function around some time t':

$$f(t) = (\omega_0 + \alpha t)t \approx (\omega_0 + 2\alpha t')t - \alpha t'^2 \tag{4.30}$$

We can now identify the frequency $\omega(t') = \omega_0 + 2\alpha t'$, explaining why the transition happens twice as fast as we first expected. This means that the effective driving speed is twice the one of the frequency driving speed. Modifying our LZ formula to reflect this doubling in speed, we get:

$$P = P_{LZ} = \exp(-2\pi a) \tag{4.31}$$

$$a = \frac{\delta_1^2}{2\alpha} = \frac{[\delta J_1(\frac{A}{\Delta})]^2}{2\alpha} \tag{4.32}$$

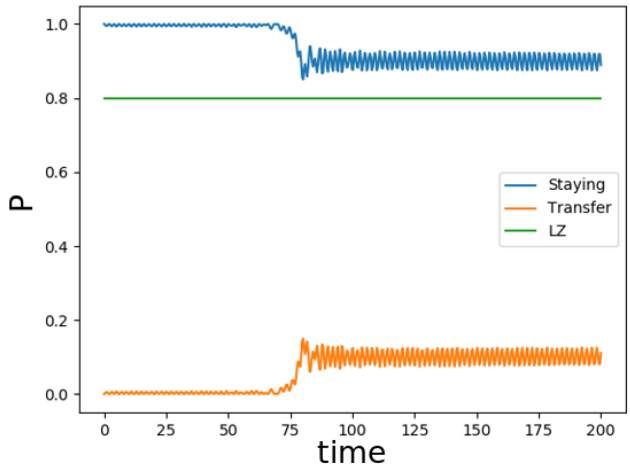

Figure 4.6: Numerical simulation compared to the first LZ probability we find. With the parameters A=3,$\delta = 2$, $\Delta = 50$, $\alpha = 0.1$ and the starting frequency $\omega_0 = 35$

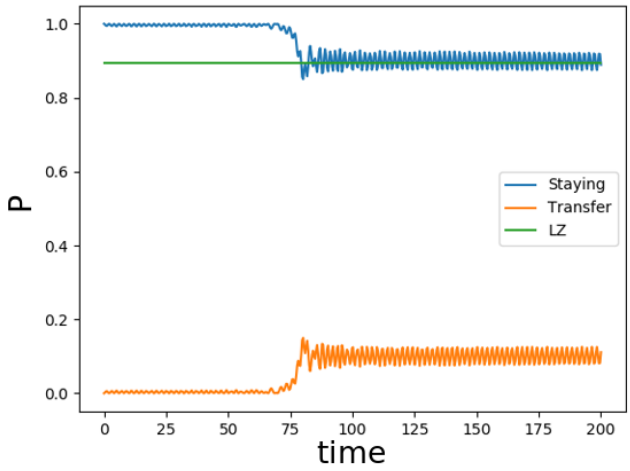

Figure 4.7: Simulation of a TLS where one level is oscillating with linearly increasing frequency compared to the RWA using the LZ formula. With the parameters A=3,$\delta = 2$, $\Delta = 50$, $\alpha = 0.1$ and the starting frequency $\omega_0 = 35$

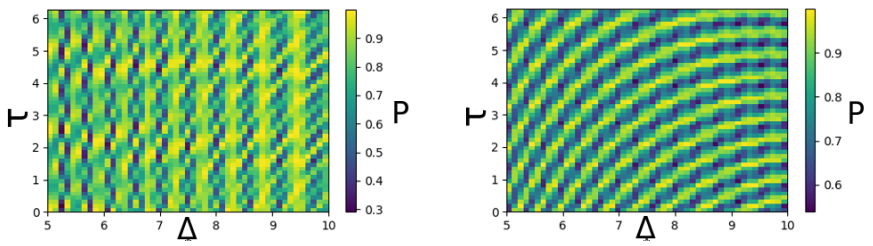

Figure 4.8: Numerical simulation giving return probability, P, as a function of level splitting and wait time, FM driven system on the left and directly driven system to the right. The directly driven system with paramaters: $\epsilon = 15$, $\delta = 0.5$, v = 0.7, xi = 10 . The FM driven level with paramaters: ω_0 = 35,v = 0.35, $\epsilon = 50$, A = 10, $\delta = \epsilon/A$, ξ = 10. ξ is how far above the upper of the two stationary levels the sweep goes. The parameters of the two system are chosen such that the coupling and the speeds of the level crossings are roughly the same.

Which is agrees with the numerical simulations, figure 4.7, where we do the same LZT as in figure 4.6. We now have a understanding of how to drive these sidebands and how the LZT looks when we cross a sideband with an energy level. What this means is that we can use the sidebands in the same way that we would have used the original levels, with new effective couplings, at least as a good approximation of what is happening. This gives us a lot of freedom, and lets us do things that would otherwise be difficult or impossible.

Comparing the return probabilities of frequency driven system to the directly driven system in the color plot in figure 4.8, we see that these systems behave quite differently, and it is not just a phase shift to make them similar. And so we cannot use the analytic result we got to describe this system accurately. It looks like there is to much fluctuations in the signal, introduced by frequency driving, and so single shot measurements with this method might be difficult. If one where to do a range of measurements with different τ, you could Fourier transform the return probability as a function of τ of these measurements, but doing enough measurements would as we mentioned be time consuming. Understanding the detailed time-dependence of the frequency driven trapezoid sweep thus requires more work, which is beyond the scope of this thesis.

4.2 Indirect Rabi oscilliations

We move on to another approach, still utilizing all of the three triplet ground states. Namely indirect Rabi oscillation, that is inducing Rabi oscillations between the two upper levels of the system by oscillating the lower level of the system. We model the system with a Hamiltonian that has no coupling between the two upper levels and having generally two different couplings to the third lower level. In the system we are modeling these two couplings are the same, but

for this calculation we will keep them different for generality.

$$H = \begin{bmatrix} E_1 & 0 & \delta_1 \\ 0 & E_2 & \delta_2 \\ \delta_1 & \delta_2 & -\epsilon_0 \end{bmatrix} \tag{4.33}$$

We want the system to begin in the $|-1\rangle$ state. The system can be initialized in different ways, but staying within the topic of LZT we can imagine that the system starts in the $|0\rangle$ level (something that is easy to do with the NV-centers), and that we use a nearly adiabatic photon-assisted level crossing to transfer the system into the $|-1\rangle$ state. After the initialization, periodic driving of the energy of the $|0\rangle$ state is turned on. The idea is that even though the two upper levels are not coupled with each other they are coupled with the oscillating level. As we saw in the previous chapter, introducing oscillations in the system with the natural frequency of the system starts Rabi oscillations. We expect the same to happen here between the two upper levels, even though they are not coupled or oscillating. We are going to start describing the system without periodic driving first, to find the effective coupling between the two upper levels.

We assume δ_1 and δ_2 to be small compared to the distance between the two upper levels and the lower level, $\delta_{1,2} \ll \epsilon_0 + E_{1,2}$ so that we can block-diagonalize the Hamiltonian pertubativly using a Schrieffer-Wolff transformation, see appendix A for details. Intuitively we see that even though the two upper levels are not coupled, they are both coupled to the lower level, and so they are indirectly coupled. The general idea is that we find a transformation that transforms the Hamiltonian to a block diagonal form up to some order in the off-(block-)diagonal elements. And by this splitting the system into the two disconnected subsystems, in this case the two upper levels from the lower level. The transformation needed to this is $U_{SW} = e^S \approx 1 + S$, where S is:

$$S \approx \begin{bmatrix} 0 & 0 & \frac{\delta_1}{E_1+\epsilon_0} \\ 0 & 0 & \frac{\delta_2}{E_2+\epsilon_0} \\ -\frac{\delta_1}{E_1+\epsilon_0} & -\frac{\delta_2}{E_2+\epsilon_0} & 0 \end{bmatrix} \tag{4.34}$$

This gives a correction to the unperturbed H_0 (which is the diagonal part of H). $\tilde{H} \approx H_0 + \frac{1}{2}[S, V]$ (where V is the off-block-diagonal part of H)

$$\frac{1}{2}[S,V] = \begin{bmatrix} \frac{\delta_1^2}{E_1+\epsilon_0} & \frac{\delta_1\delta_2}{2}\left(\frac{1}{E_1+\epsilon_0} + \frac{1}{E_2+\epsilon_0}\right) & 0 \\ \frac{\delta_1\delta_2}{2}\left(\frac{1}{E_1+\epsilon_0} + \frac{1}{E_2+\epsilon_0}\right) & \frac{\delta_2^2}{E_2+\epsilon_0} & 0 \\ 0 & 0 & -(\frac{\delta_1^2}{E_1+\epsilon_0} + \frac{\delta_2^2}{E_2+\epsilon_0}) \end{bmatrix} \tag{4.35}$$

Calling this matrix β, we can then write the block-diagonalized Hamiltonian:

$$\tilde{H} \approx \begin{bmatrix} E_1 + \beta_{11} & \beta_{12} & 0 \\ \beta_{21} & E_2 + \beta_{22} & 0 \\ 0 & 0 & -\epsilon + \beta_{33} \end{bmatrix} = \begin{bmatrix} \tilde{E_1} & \beta_{12} & 0 \\ \beta_{21} & \tilde{E_2} & 0 \\ 0 & 0 & -\tilde{\epsilon_0} \end{bmatrix} \tag{4.36}$$

Next we introduce the periodic driving, $A\cos(\omega t)\,|3\rangle\langle 3|$. We introduce this term as a small

perturbation, $f = A\cos(\omega t)$, to ϵ_0. The terms $\beta_{12,21}$ then becomes:

$$\begin{aligned}\beta'_{12,21} &= \frac{\delta_1\delta_2}{2}\left(\frac{1}{E_1+\epsilon_0+f}+\frac{1}{E_2+\epsilon_0+f}\right)\\ &\approx \frac{\delta_1\delta_2}{2}\left(\left(\frac{1}{E_1+\epsilon_0}+\frac{1}{E_2+\epsilon_0}\right)-f\left(\frac{1}{(E_1+\epsilon_0)^2}+\frac{1}{(E_2+\epsilon_0)^2}\right)+\mathcal{O}(f^2)\right)\\ &= \beta_{12,21}-f\chi_{12,21}+\mathcal{O}(f^2)\end{aligned} \tag{4.37}$$

And similarly for the $\beta_{11,22}$ terms:

$$\begin{aligned}\beta'_{11,22} &\approx \delta_{1,2}^2\left(\frac{1}{E_{1,2}+\epsilon_0}+\frac{f}{(E_{1,2}+\epsilon_0)^2}+\mathcal{O}(f^2)\right)\\ &= \beta_{11,22}-f\chi_{11,22}+\mathcal{O}(f^2)\end{aligned} \tag{4.38}$$

Where we have given the new terms introduced by the perturbation the name χ. We have separated the two subsystems up to first order and reintroduced the driving term. We focus on the subsystem of the two upper levels from now on. The full approximated Hamiltonian is then:

$$H_{TLS} = \begin{bmatrix}\tilde{E}_1-\chi_{11}A\cos(\omega t) & \beta_{12}-\chi_{12}A\cos(\omega t)\\ \beta_{12}-\chi_{12}A\cos(\omega t) & \tilde{E}_2-\chi_{22}A\cos(\omega t)\end{bmatrix} \tag{4.39}$$

This looks similar to earlier examples with oscillating levels and couplings, we have effectively found both longitudinal and transverse driving in the system. The way we treated this was by applying a transformation to a rotating reference frame, moving the time dependence to the off-diagonal, then using the rotating wave approximation. The first step is to find the transformation that will move the oscillating terms:

$$U = \begin{bmatrix}e^{-i\chi_{11}\frac{A}{\omega}\sin(\omega t)} & 0\\ 0 & e^{-i\chi_{22}\frac{A}{\omega}\sin(\omega t)}\end{bmatrix} \tag{4.40}$$

We can then apply this transformation to the Schrödinger equation, as we have done earlier. This will give us a transformed Hamiltonian:

$$\tilde{H}'_{TLS} = \begin{bmatrix}\tilde{E}_1 & \xi\\ \xi^* & \tilde{E}_2\end{bmatrix} \tag{4.41}$$

$$\xi = (\beta_{12}+\chi_{12}A\cos(\omega t))\exp\{i\frac{(\chi_{22}-\chi_{11})A}{\omega}\sin(\omega t)\} \tag{4.42}$$

We recognise this complex exponential with a sine function, we can simplify by using the Bessel function identity, eq. (3.9). Applying this to ξ we get:

$$\begin{aligned}\xi &= (\beta_{12}+\chi_{12}A\cos(\omega t))\sum_n J_n\left(\frac{(\chi_{22}-\chi_{11})A}{\omega}\right)e^{in\omega t}\\ &= \beta_{12}\sum_n J_n\left(\frac{(\chi_{22}-\chi_{11})A}{\omega}\right)e^{in\omega t}\\ &+ \chi_{12}\frac{A}{2}\sum_n J_n\left(\frac{(\chi_{22}-\chi_{11})A}{\omega}\right)\left(e^{i(n-1)\omega t}+e^{i(n+1)\omega t}\right)\end{aligned} \tag{4.43}$$

The coupling is now three infinite sums of harmonics. We are now going to apply the RWA, since we are going to look at the case of driving close to the resonance between the two upper levels. We introducing a rotating reference frame on the form:

$$V = \exp\{\frac{ik\omega t}{2}\sigma_z\} \tag{4.44}$$

Since we are assuming that $\omega \approx E_1 - E_2$ we set $k = 1$. This gives us the Hamiltonian:

$$(\tilde{H}'_{TLS})_{RW} = \begin{bmatrix} \tilde{E}_1 - \frac{\omega}{2} & \xi e^{-i\omega t} \\ \xi^* e^{i\omega t} & \tilde{E}_2 + \frac{\omega}{2} \end{bmatrix} \tag{4.45}$$

$$\begin{aligned} \xi e^{-i\omega t} = \beta_{12} \sum_n J_n \left(\frac{(\chi_{22} - \chi_{11})A}{\omega} \right) e^{i(n-1)\omega t} \\ + \chi_{12} \frac{A}{2} \sum_n J_n \left(\frac{(\chi_{22} - \chi_{11})A}{\omega} \right) \left(e^{i(n-2)\omega t} + e^{in\omega t} \right) \end{aligned} \tag{4.46}$$

The next step in the RWA is the approximation, we are going to ignore everything that is still oscillating, discarding fast oscillating terms as well as counter rotating terms, keeping only terms that are oscillating with relevant energies.

$$\begin{aligned} (\xi e^{-i\omega t})_{RWA} = \beta_{12} J_1 \left(\frac{(\chi_{22} - \chi_{11})A}{\omega} \right) \\ + \chi_{12} \frac{A}{2} \left(J_2 \left(\frac{(\chi_{22} - \chi_{11})A}{\omega} \right) + J_0 \left(\frac{(\chi_{22} - \chi_{11})A}{\omega} \right) \right) \end{aligned} \tag{4.47}$$

Applying the RWA has simplified the Hamiltonian a great deal, but we can do even better. We are working to second order in the coupling elements, the χ and β elements are second order in the couplings, $\beta_{\mu\nu} \propto \delta_\mu \delta_\nu$ and $\chi_{\mu\nu} \propto \delta_\mu \delta_\nu$. The arguments of the Bessel functions are therefor small, low order Taylor expansion is therefor a good approximation. For small x:

$$J_0(x) \approx 1 - \frac{x^2}{4} \tag{4.48}$$

$$J_1(x) \approx \frac{x}{2} \tag{4.49}$$

$$J_2(x) \approx \frac{x^2}{8} \tag{4.50}$$

We need to be a bit careful, even though β and χ is the same order in the couplings, β is quite a bit larger by a factor $\approx \epsilon_0$. If we compare the highest order terms of the first and last term in eq. (4.47) we see that the ratio of these are $\approx \frac{\delta^2}{\epsilon_0 \omega}$. And since $\epsilon > \omega \gg \delta$, we see that even though β is larger, this is not enough to make them comparable. We can therefor simplify by just keeping terms of order $\mathcal{O}(\delta^2)$:

$$(\xi e^{-i\omega t})_{RWA} \approx \frac{\chi_{12} A}{2} \tag{4.51}$$

Giving us the Hamiltonian:

$$\tilde{H}_{RWA} = \begin{bmatrix} \tilde{E}_1 - \frac{\omega}{2} & \frac{\chi_{12} A}{2} \\ \frac{\chi_{12} A}{2} & \tilde{E}_2 + \frac{\omega}{2} \end{bmatrix} \tag{4.52}$$

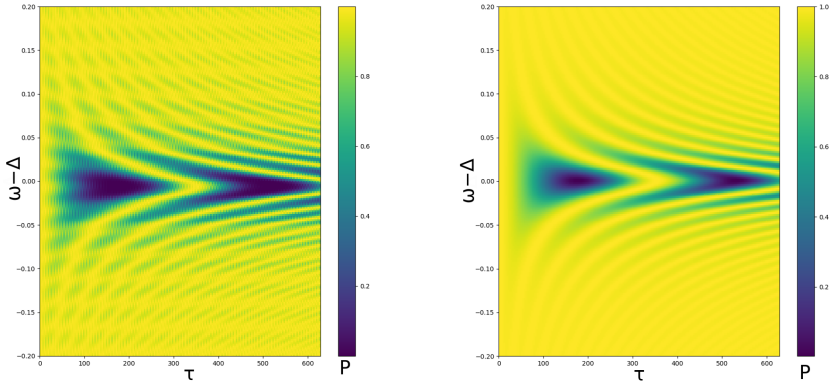

(a) **(b)**

Figure 4.9: Plots of return probability as a function of frequency detuning ($\omega - \Delta$) and driving time (τ) under indirect Rabi oscillation like desribed in 4.2 with the zero field splitting $E_1 + \epsilon = 50$, level splitting of $E_1 - E_2 = 5$ and a coupling $\delta_1 = \delta_2 = 2$ and a driving amplitude of $A = 10$, (a) is plot of simulation, while (b) is the a plot of the analytic result above.

The Hamiltonian is now very much simplified and we have removed any explicit time dependence. There is still a time dependence in the reference frame, but the occupation probabilities are going to be the same in the rotating and the stationary frame. From the Hamiltonian we see that we get Rabi oscillations at $\omega = \tilde{E}_1 - \tilde{E}_2 \approx E_1 - E_2 = \Delta$, with Rabi frequency $\Omega_R = \frac{\chi_{12} A}{2}$ at resonance, as we mentioned in 3.2.1.

The analytic approximation of the return probability is then

$$P(\tau) = 1 - \frac{|\delta'|^2}{\frac{1}{4}\Delta^2 + |\delta'|^2} \sin^2\left(\sqrt{\frac{1}{4}\Delta^2 + |\delta'|^2}t\right) \tag{4.53}$$

Where $\delta = \frac{\chi_{12} A}{2}$ and $\Delta = E_1 - E_2$. This is compared to the simulation of the system, obtained by using the code in appendix B, in figure 4.9. As we can see there is good correspondence between the simulated result and the analytic result we found. We see some oscillations that comes from the way we are driving this system.

4.2.1 Measurement

A measurement of the level splitting and hence the magnetic field can then be preformed by running the experiment described in the section above. We could then employ the single-shot measurement that we talked about for the trapezoid method, singling in on a point near resonance, but this would of course be vulnerable to the same noise that that appears due to the indirect driving. However we can do the experiments for different driving frequencies. This will give us a vertical cross section of figure 4.9a. We can then use the symmetry around the resonance to find it.

Chapter 5

Quantum mechanical treatment of driving: coupling to a photon field

Up to this point we have taken a classical approach to driving, by driving the energy of the states. As we will see this is just the classical limit of the fully quantum driving we will look at in this chapter. Also we have talked about photon sidebands, up til now acquired by a transformation trick. The justification for calling them photon sidebands has maybe been a bit thin, drawing the connection between the theory we have presented and the one we are going to present is going to justify this. When looking into how the photons affects the level crossings, another very interesting question is what happens to the photons when we have level crossings. The semi-classical approach does not take into account what happens to the driving field. Describing the driving in a classical way, makes the driving just a parameter in the theory so there is no way to describe how the coupling affects the field. But if we take the quantum mechanics of the driving field seriously and look at the limit of large numbers of photons and the case of coherent states, a type of state we will define later, we will see that this overlaps with the classical picture we have looked at in the previous chapter. We therefore expect that the effect on the field in this limit also is minimal. However if we look at smaller photon numbers and/or other states of the field, we expect to find that level crossings also affect the field.

What we will look at in this chapter is a model of a system with a single photon mode coupled to a TLS. We will modify this model slightly in the following sections and chapters. We are going to need some new tools to be able to represent what state the system in, so we introduce two visual methods for showing the system state. After presenting the model we show that this is indeed describing the same systems as we have been looking at in previous chapters, when taking the classical limit.

5.1 TLSs coupled to a photon mode

Our starting point for the analysis of this problem is the Hamiltonian describing a TLS with coupling to a single photon mode:

$$\hat{H} = \omega \hat{a}^\dagger \hat{a} + \Delta \frac{\hat{\sigma}_z}{2} + A\left(\hat{a} + \hat{a}^\dagger\right)\sigma_x. \tag{5.1}$$

Where the a operators are the photon creation and annihilation operators, and $\hat{N} = \hat{a}^\dagger \hat{a}$ is the photon number operator. This Hamiltonian describes a TLS with a level splitting Δ, that allows for transfer from one level to another by emission/absorption of a photon with the frequency ω. This is what we will call transverse driving, again because of the driving term including σ_x. Notice that the two levels are only coupled via this photon interaction and the similarities with the transverse classical driving. A way of interpreting this system is starting out with the two level system and then imagining energy levels above each of these with energy ω between them, dressing the two states with photons. As we can see from the Hamiltonian, far away from crossings where interactions are negligible, the state has energy of the atom state that it is in (second term) plus the number of photons times the energy of a photon (first term).

The Hamiltonian described in eq. (5.1) is often simplified by introducing an approximation to get an exact solvable model. The approximation is the same as the one we talked about in the semi-classical treatment of the problem, namely the RWA, since we also here are interested in what happens around resonance. The Hamiltonian we get after applying the RWA is called the Jaynes-Cummings Hamiltonian. The model was developed by Edwin Jaynes and Fred Cummings in a 1968 article [31], to be a fully quantum mechanical description of the interaction between a TLS with a electromagnetic field. Assuming $\omega \approx \Delta$ we can approximate the Hamiltonian in eq. (5.1) as:

$$\hat{H}_{\text{JC}} = \omega \hat{a}^\dagger \hat{a} + \Delta \frac{\hat{\sigma}_z}{2} + A/2\left(\hat{a}\hat{\sigma}_+ + \hat{a}^\dagger \hat{\sigma}_-\right). \tag{5.2}$$

The Jaynes-Cummings Hamiltonian is used extensively when describing Quantum dots trapped in a photon cavity [32, 33]. It can also be used when looking at Rydberg atoms [34] or trapped ions [35]. In [36] a similar model is used to describe a double quantum dot irradiated with a probe field longitudinally.

At this point it can be useful to decide on some notation, we are going to call the atom state that starts out with the most energy "0" and the one with the least "1", then together with a photon number we can make a basis. We write the state where the system is in the "0" state and with n photons $|0\rangle \otimes |n\rangle = |0, n\rangle$.

5.2 Connection between classical driving and coupling to a photon mode

In this section we will have a look at the connection between classical driving and a fully QM Hamiltionan introduced in this chapter. This section is based on the treatment of the dressed state formalism in [37], but could also be done with Floquet theory as is done in [38].

We are going to assume a coherent light state in this section because laser light can approximated as a coherent state. If one starts out trying to find the state that balance the uncertainty

in the two canonically conjugate variables, photon number and phase one will end up with the coherent state. Another way to find the coherent state is to find the solution to the quantum harmonic oscillator, and if you displaces this state from the center you get oscillating behaviour like in the classical harmonic oscillator. The coherent state is therefore the go to solution when we see oscillating behaviour in a quantum system. When solving the quantum harmonic oscillator it is common to introduce creation and annihilation operators that take you from one solution to the next (ladder operators), and in this case we see that another way of defining the coherent state is that it is the eigenstates of the bosonic creation and annihilation operator:

$$a\left|\alpha\right\rangle = e^{-i\omega t}\alpha_0\left|\alpha\right\rangle \tag{5.3}$$

All in all the coherent state is the most classical state we can produce at a quantum level. We can express coherent states in terms of number states, which are states that have well defined number of particles, these states are also known as Fock states.

$$\left|\alpha\right\rangle = e^{-\frac{|\alpha|^2}{2}}\sum_{n=0}^{\infty}\frac{\alpha^n}{\sqrt{n!}}\left|n\right\rangle = \sum_{n=0}^{\infty}c_n\left|n\right\rangle \tag{5.4}$$

We can write the fully quantum mechanic Hamiltonian from eq. (5.1) as a sum of the atom energy, the energy of the photons and the interaction part:

$$H_{QM} = H_e + H_p + V_i \tag{5.5}$$

Where the two first terms in the Hamiltonian are given by:

$$H_e = \left(E_0\left|0\right\rangle\left\langle 0\right| + E_1\left|1\right\rangle\left\langle 1\right|\right)\otimes I_p \tag{5.6}$$

$$H_p = \omega a^\dagger a \otimes I_e \tag{5.7}$$

These are the atom and the photon Hamiltonian respectively, where a is the photon annihilation operator. V_i, the interaction, is defined as in the JC Hamiltonian:

$$V_i = V_e \otimes (a^\dagger + a) \tag{5.8}$$

To identify what V_e needs to be in order for the classical and quantum case to be similar, we use the classical correspondence principle and the assumption that we are working with coherent states. As we mentioned the coherent state is an eigenstate of the creation and annihilation operator:

$$a\left|\alpha\right\rangle = e^{-i\omega t}\alpha_0\left|\alpha\right\rangle \tag{5.9}$$

And so we can find the matrix element given by:

$$\left\langle\alpha\right| V_i\left|\alpha\right\rangle = V_e(\alpha_0^* e^{i\omega t} + \alpha_0 e^{-i\omega t}) \tag{5.10}$$

$$= 2|\alpha_0|V_e\cos(\omega t + \phi) \tag{5.11}$$

We can then make the identification $|\alpha_0|V_e = A/2\sigma_{x,z}$, for the case of transverse and longitudinal driving respectively. For simplicity we set $\phi = 0$. Finally we want to evaluate H_{QM} in the $\{|i,n\rangle\}$ basis, again using that the field is in a coherent state:

$$\left\langle i,m\right| V_e a^\dagger\left|j,n\right\rangle = \left\langle i,m\right| V_e\sqrt{1+n}\left|j,n+1\right\rangle \tag{5.12}$$

$$\approx \left\langle i\right| V_e\left|j\right\rangle\alpha_0\delta_{m,n+1} \tag{5.13}$$

$$= \frac{V_{ij}}{2}\delta_{m,n+1} \tag{5.14}$$

Where the δ in this expression is the Kronecker delta. We can find the $V_e a$ term in the same manner, giving us:

$$\langle i,m|\, V_e a\, |j,n\rangle = \frac{V_{ij}}{2}\delta_{m+1,n} \tag{5.15}$$

For the two other terms in the Hamiltonian:

$$\langle i,n|\, H_e\, |j,m\rangle = E_i\delta_{i,j}\delta_{n,m} \tag{5.16}$$

$$\langle i,n|\, H_p\, |j,m\rangle = n\omega\delta_{i,j}\delta_{n,m} \tag{5.17}$$

The whole Hamiltonian, H_{QM}, can now be written on a tri-block-diagonal form, that is with 2×2 blocks on a tri-diagonal form. In the case of driving of one of the levels, what we have called longitudinal driving, we have $V_{01} = V_{10} = V_{00} = 0$ and $V_{11} = A$. While the transverse driving would be represented by $V = A\sigma_x$. As an example lets have a look at longitudinal driving in the case where the driving field is in a coherent state. The Hamiltonian is then:

$$H_{QM} = \begin{bmatrix} \ddots & & & & & \\ & E_1+(n-1)\omega & 0 & A/2 & 0 & 0 & \\ & 0 & E_0+n\omega & 0 & 0 & 0 & \\ & A/2 & 0 & E_1+n\omega & 0 & A/2 & \\ & 0 & 0 & 0 & E_0+(n+1)\omega & 0 & \\ & 0 & 0 & A/2 & 0 & E_1+(n+1)\omega & \\ & & & & & & \ddots \end{bmatrix} \tag{5.18}$$

As we would expect the E_0 levels are not coupled to anything, and so if we put it in one state it will stay there. We can therefor simplify the Hamiltonian by only keeping one of these levels, $E_0 + n\omega$, where $n = 0$. This gives:

$$H_{QM} = \begin{bmatrix} E_0 & & & & \\ & \ddots & & & \\ & & E_1+(n-1)\omega & A/2 & 0 & \\ & & A/2 & E_1+n\omega & A/2 & \\ & & 0 & A/2 & E_1+(n+1)\omega & \\ & & & & & \ddots \end{bmatrix} \tag{5.19}$$

What we have done is removing the time dependence of the problem, at the cost of re expressing the problem in an infinite dimensional Hilbert space. While the coherent states are a superposition of many number states, the distribution is in this case narrowly peaked around the expected photon number. This is another property of coherent states, the photons are distributed according to the Poisson distribution, and so the relative width of the distribution in Fock space gets thinner and thinner the bigger the coherent state is. So in the limit of expectation of infinite photon number, the distribution is just a delta function centered at the expected photon number. We can therefore look at a small portion of this Hamiltonian, the portion with $n \simeq \alpha^2$. As we see from eq. (5.18) we have now re expressed the system as a two level system, where in this case one of them is "dressed" with photons. In the classical limit there are a lot of photons present so we are looking at the states around some big n. Meaning that we have photon states both above and bellow as we have seen.

5.3 Schrödinger cat states

States that come up quite a bit in these types of systems are known as Schrödinger cat states or just cat states. The reason they are called that, is that they are superpositions of somewhat classical states, like the case of the cat in Schrödingers gedanken experiment, where a cat is in an superposition of being alive and dead. As we mentioned in the section above, the closest we get to classical states are coherent states, when working with photons. We are going to look at a superposition of two coherent states with amplitude α and $-\alpha$, where the amplitude is equal for both of them, but generally not having the same phase.

$$\psi = (|\alpha\rangle + e^{i\phi}|-\alpha\rangle)/N_\phi \tag{5.20}$$

Some special cases that we will be using in this thesis are:

- The even state ($\phi = 0$): Only even Fock states are occupied.
- The odd state ($\phi = \pi$): Only odd Fock states are occupied.
- The Yurke-Stoler state ($\phi = \pi/2$): Poisson distribution in Fock space.

These types of states have a wide variety of use cases, they have been found to be useful in meteorology as an alternative to so called NOON states [39] and for sensitive force detection [40], quantum information processing [41] and quantum teleportation [42]. It has been shown that these coherent superpositions can be used as qubits and only need linear optics to do the operations needed to make a quantum computer [41], but making the states in the first place is usually taken as a initial requirement. We will come back to how this might be possible with photon assisted LZT in the end of this thesis. Sending quantum information with these states would also be good as it would be fast and reliable, since light has good coherence properties [43], but what we will be looking at in later chapters is manipulating these states. One could imagine using the even and odd states as binary states, "0" and "1" in a quantum computer, what is known as a qubit [44]. This choice of states would make the *measurement* of a qubit easy. You just measure the number of photons, if you measure an even (odd) number of photons, you know you are in say the "0" ("1") state. One other advantage of using these superpositions over only coherent states is that even and odd coherent states are actually orthogonal, while $|\alpha\rangle$ and $|-\alpha\rangle$ are only almost orthogonal.

$$\begin{aligned}\langle\alpha|-\alpha\rangle &= \left(e^{-\frac{|\alpha|^2}{2}}\sum_{m=0}^{\infty}\frac{\alpha^m}{\sqrt{m!}}\langle m|\right)\left(e^{-\frac{|\alpha|^2}{2}}\sum_{n=0}^{\infty}\frac{\alpha^n}{\sqrt{n!}}|n\rangle\right)\\ &= e^{-|\alpha|^2}\sum_{m=0}^{\infty}\frac{(-\alpha^2)^n}{n!}\\ &= e^{-2|\alpha|^2}\end{aligned} \tag{5.21}$$

However there are also drawbacks by using even and odd states, they are very sensitive to photon loss and detection inefficiency. There are however more complicated schemes that still uses these cat states that are not so sensitive to these error sources [45], but we will not go into detail on these.

5.4 Visualisation

One of the advantages of the FLSs discussed in the previous section was their simplicity. By giving the amplitudes of each of the levels, we had a full understanding of what state the system was in. Now however things are more complicated. We have to keep track of a photon field as well. We need some way of visualizing what is going on. Keeping our graphs that tell us the probability of being in each of the atom states, and introducing two new types of visualisation.

The first is pretty intuitive, probability of the system being in each of the number states, showing the distribution in Fock space. The advantage of this is that it gives a clear overview of the probabilities of each number state, making it easy to distinguish some states but on the other hand information about phase is lost. The other is more abstract. We are going to use something referred to as a quasi-probability distribution, the number/phase Wigner quasi-probability distribution to be precise. The Wigner distribution for a density matrix, ρ, for momentum and position is defined as:

$$W(x,p) = \frac{1}{\pi}\int_{-\infty}^{\infty} \langle x+y|\hat{\rho}|x-y\rangle e^{-2ipy}\, dy, \tag{5.22}$$

Where $\langle x|\psi\rangle = \psi(x)$ is the position wave function and x and p are position and space. This function has many of the properties of a probability distribution, e.x. that integrating over the position gives us the momentum spectrum:

$$\int_{-\infty}^{\infty} dp\, W(x,p) = \langle x|\hat{\rho}|x\rangle \tag{5.23}$$

The number and phase version of this function is more convoluted to defined as we can see in [46], but the idea is the same. In these plots, number is given as the radial component, while phase is given as the angle. The Wigner distribution is a probability-like function that tries to represent the probabilities of two canonical variables at the same time. This is not possible to do of course due to the uncertainty principle, which is why the quasi-probability is not an actual probability. The quasi-probability can be negative, generally indicating that there is something non-classical about the state. The advantage of this method is that it shows the nature of the underlying state better.

As an example we have illustrated a cat state in these two ways in fig 5.1, the state presented is a even state. We will be using a combination of these two, in addition to the transfer probability when needed, to give a picture of what state the system is in. As a quick note: a simple coherent state is represented by a single diffuse disk off center, without any fringes or negative values, shown in figure 5.1c. This also builds upon what we know about coherent states, we can see that it has the same uncertainty in number and phase since it is round. It also has a non negative Wigner function, which points to the classical nature of the coherent state.

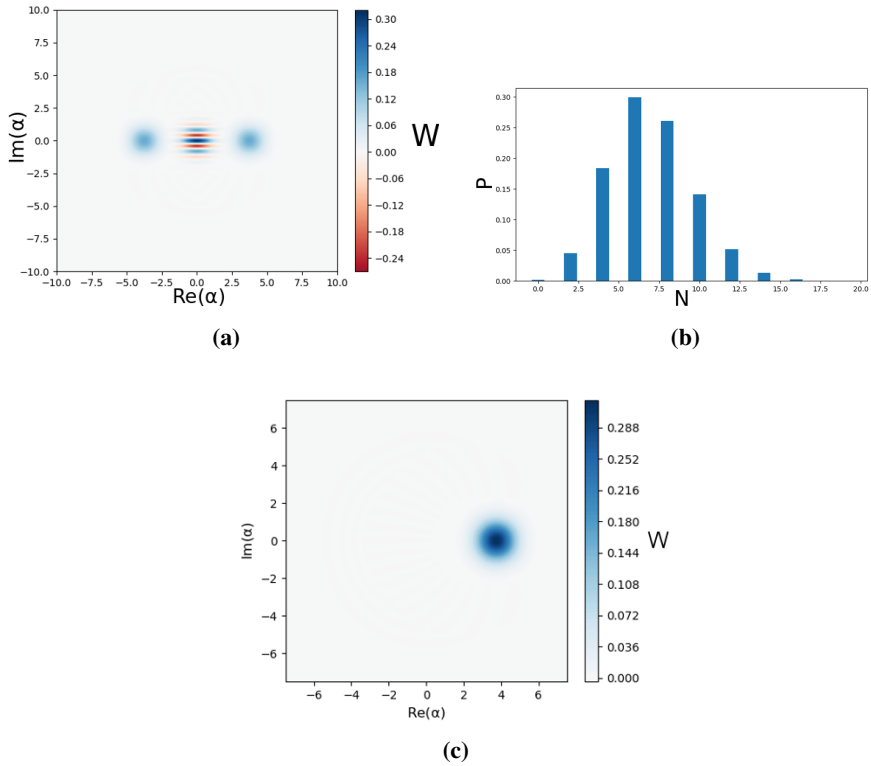

Figure 5.1: Example of a Fock distribution (b) and a Wigner distribution (a), of a superposition of coherent states. In (c) the Wigner function of a coherent state is shown.

Chapter 6

Photon assisted Landau Zener transitions under QM driving

In this chapter we are going to take a look at what happens when we have avoided level crossings, Landau-Zener transitions, in the types of model introduced in the last chapter. Analogous to the case of classical driving, we expect to see photon assisted Landau-Zener transitions. As in the case of classical driving, we will have a look at both transverse and longitudinal driving during the LZ sweep.

6.1 Landau-Zener transitions with coupling to a photon mode

The modification we will make to the Hamiltonian in eq. (5.1) is to introduce driving of the level splitting.

$$\hat{H} = \omega \hat{a}^\dagger \hat{a} + (\Delta - vt)\frac{\hat{\sigma}_z}{2} + A\left(\hat{a} + \hat{a}^\dagger\right)\sigma_x \tag{6.1}$$

Which we will continue to analyze in the following section and chapters in the case of small couplings, that is when the crossings are well separated so that we can treat them as separate events.

6.2 Effects on the photon field

As stated, one of the reasons to look at the Hamiltonian presented in this chapter and the last was that we wanted to have a look at how LZTs affect the photon field. We don't only care about the total probability of the system moving from one atom level to another, we also care about how the photon field is affected by a level crossing. To see how the photon state changes we will first look at a method where a single parameter shows how the distribution changes, and then in the next chapter we will have a more detailed look, presenting the probabilities of being in different Fock states during a LZTs as well as Wigner distributions.

6.3 Transverse driving: Landau Zener transitions with photon states

We have a good picture of how LZT looks like with the classical driving, even the crossing of the sidebands. In this section we will look at how LZT looks like with the Hamiltonian presented in eq. (6.1). First we will have a look at the interaction term in the Hamiltonian. We look at how the creation (annihilation) operator acts on number states:

$$a\,|s,n\rangle = \sqrt{n}\,|s,n-1\rangle \tag{6.2}$$

$$a^\dagger\,|s,n\rangle = \sqrt{n+1}\,|s,n+1\rangle \tag{6.3}$$

As we can see this creates off-diagonal elements in photon space, such that there is coupling between neighboring photon states with a factor $\sqrt{n}$ in addition to the coupling strength, where n is photon number of the upper of the two coupled levels. In the case of the Hamiltonian in eq. (6.1) the photon level, n, is coupled to the neighboring energy levels, $n \pm 1$, in the other atom level because of the transverse coupling σ_x. The LZ probability is therefore dependent on what photon state the system is in.

Keeping to the number states we look at how a single crossing looks like. Initializing the system in the $|0,n\rangle$ state and having it cross the $|1,n+1\rangle$ level by driving the TLS energy levels like in eq. (6.1). The coupling between the states is as we found above:

$$\langle 0,n|\,H\,|1,n+1\rangle = A\sqrt{n+1} \tag{6.4}$$

And so the probability of transfer is:

$$P_{LZ}^{(n)} = e^{-2\pi A^2(n+1)/v} \tag{6.5}$$

This is rigorously shown in [47], where they derive the LZ probability from the Hamiltonian above. As we can see, the coupling and hence the transfer probability is dependent on which photon state we are looking at and is increasing with rising photon numbers.

We now know how a single number state LZT look like, but generally we have access to or want to work with more intricate states. The go to photon state is the coherent state. We will therefore use this to show how we work with these more complicated photon states, but the method is general. We look at the state as a sum of number states

$$|\alpha\rangle = e^{-\frac{|\beta|^2}{2}} \sum_{n=0}^{\infty} \frac{\alpha^n}{\sqrt{n!}}\,|n\rangle = \sum_{n=0}^{\infty} c_n\,|n\rangle \tag{6.6}$$

The total LZ probability, that is the probability to go from $|0\rangle$ to $|1\rangle$ (or the other way around), is then a sum over all the number state transfer probabilities weighted with the coefficients c_n:

$$P_{LZ} = \sum_{n=0}^{\infty} |c_n|^2 P_{LZ}^{(n)} \tag{6.7}$$

This is just the atom level probabilities however, the effects on the photon field can be a bit more complicated. In [47] this is investigated using the cat states that we mentioned in section 5.3.

In this paper they mainly focus on how the cat states affects the LZ probability, but they also investigate what happens to the photon field. The way that they measure how much the photon state has changed is by calculating something called the Q parameter introduced by Mandel in [48]:

$$Q = \frac{(\Delta n)^2}{\bar{n}} - 1 \tag{6.8}$$

Where $(\Delta n)^2$ is the variance of the number operator and $\bar{n} = \alpha^2$ is the mean photon number. The Q parameter is a measure of departure from the Poissonian distribution, or how far it is from being "classical". When $Q = 0$ the state is what we call Poissonian, the coherent state and the YS state being examples of two such states. While the even state is what is called super-Poissonian since $Q > 0$, while an odd is sub-Possonian, since $Q < 0$. They among other things point out that in the case of large α^2 the resulting Q paramater after LZT is unchanged, meaning that the photon distribution is unaffected which fits well with the picture of the classical driving.

6.4 Longitudinal driving

We are now going to make another modification to the Hamiltonian describing LZT in a TLS coupled to a photon mode we looked at in eq. (6.1). In this chapter we are going to have a look at the case of LZT with longitudinal coupling to the photon field, instead of the transverse coupling in the sections above. We then have the Hamiltonian:

$$H = (\omega_0 - vt)\left|0\right\rangle\left\langle 0\right| + \omega a^\dagger a - A\left|1\right\rangle\left\langle 1\right|(a + a^\dagger) - \delta(\left|0\right\rangle\left\langle 1\right| + \left|1\right\rangle\left\langle 0\right|) \tag{6.9}$$

Where ω_0 is the original splitting, v is the level driving speed and ω is the photon frequency. A and δ are coupling strengths. A version of this system is investigated in [36], where they look at a double quantum dot in an optical cavity irradiated by a probe field longitudinally. Notice that we have a time independent coupling between the levels since we need some coupling between the two levels for level crossings to be non-trivial. In this case there is coupling between the photon sidebands of one of the levels, as we saw when we looked at the dressed state formalism. We saw in the classical case that the system is fairly similar to the case of transverse driving, but one big difference is that there is not just two possible crossings anymore, there are infinitely many, as we can see in figure 6.1. The levels are not directly coupled, but as we will see they are indirectly coupled like in section 4.2. We will use perturbation theory to find how strongly they are coupled.

The effective coupling is heavily damped for most of the crossings, depending on ratio of the coupling strength A and the frequency of the mode ω. We can see this from the Hamiltonian above since only the same levels with the same photon number are directly coupled. As we saw in section 4.2, levels that have an indirect coupling via another level still have a coupling to that level, but suppressed by how far it is to that level (perturbation theory). This means that we can control the number of crossings that affect the system, and that we can have successive crossing with increasing or decreasing effective coupling. This will enable us to have more freedom in what we can do and interference effects will become more important. This formalism will give us the tools to have a look at what happens when we turn on classical longitudinal driving, using the link between the semi-classical and fully quantum Hamiltonian shown in the last chapter. After showing this, we will look into what happens in a number state LZT like we did in the

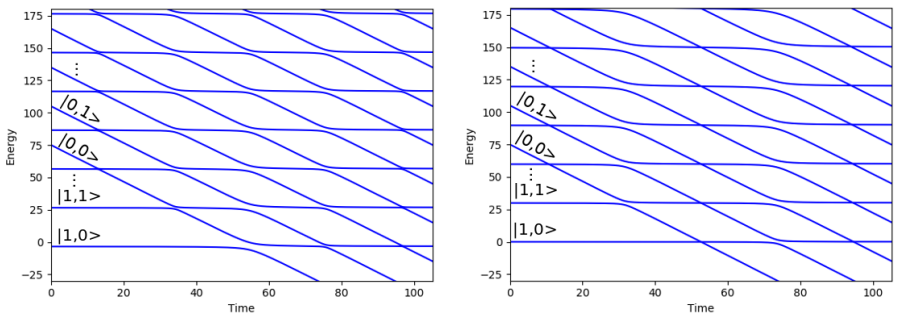

(a) **(b)**

Figure 6.1: Time dependent energy spectrum of the longitudnal (a) and transverse driving (b), without the RWA.

transverse case, but we now have more crossings to look into, first having a look at the one and zero photon transitions, and then find a general expression for multi photon processes .

6.4.1 Turning on longitudinal driving

In this section we will look at what happens when we turn on classical longitudinal driving. The idea behind this is that it will let us investigate how the photon side bands are coupled, at the same time exploring how this new formalism we have introduced can be used to solve classical driving problems. We are going to investigate a simple avoided level crossing followed by periodic driving of one of the levels, again followed by a avoided level crossing, schematically shown in an energy-time diagram in figure 6.2. We look at the case where we have a TLS, initialized in the $|0\rangle$ state, we then drive this level through the $|1\rangle$ level and then turn on periodic driving in the $|1\rangle$ level, letting the driving persist for some time τ before turning it of, and then drive the levels through each other again. We start by looking at the fully QM Hamiltonian that corresponds to classical driving with coherent states that we found in the last chapter:

$$H_{QM} = \begin{bmatrix} E_0 & & & & & \\ & \ddots & & & & \\ & & E_1 + (n-1)\omega & A/2 & 0 & \\ & & A/2 & E_1 + n\omega & A/2 & \\ & & 0 & A/2 & E_1 + (n+1)\omega & \\ & & & & & \ddots \end{bmatrix} \tag{6.10}$$

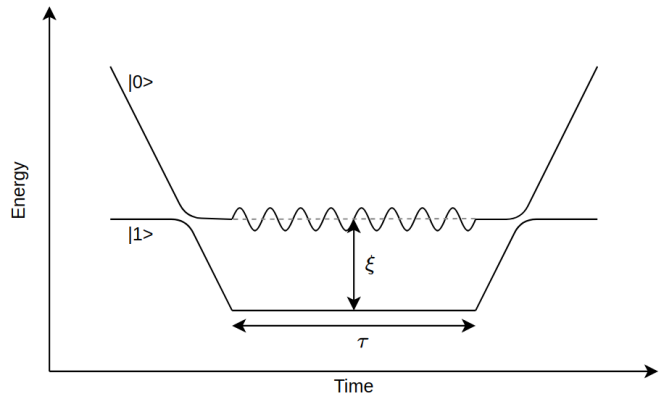

Figure 6.2: Schematical energy-time diagram showing the instantaneous energy levels in the process we investigate in section 6.4.1

Where $E_0 = 0$ and $E_1 = \xi$. We then use a Schrieffer-Wolff transformation (more details in section A) to diagonalize the E_1 part of the Hamiltonian perturbatively. To first order we get:

$$U_{SW} = \begin{bmatrix} \ddots & & & & & \\ \gamma & 1 & -\gamma & & & \\ & \gamma & 1 & -\gamma & & \\ & & \gamma & 1 & -\gamma & \\ & & & & \ddots & \end{bmatrix} \tag{6.11}$$

Where $\gamma = \frac{A/2}{\omega}$. This leaves the all the energy levels except the bottom level unchanged, $\tilde{E_1}^{(n)} = E_1^{(n)}$, but we are assuming large n so this will not affect our system. The states transforms as:

$$|\widetilde{n}\rangle = -\gamma\,|n-1\rangle + |n\rangle + \gamma\,|n+1\rangle \tag{6.12}$$

$$|n\rangle = -\gamma\,|\widetilde{n-1}\rangle + |\widetilde{n}\rangle + \gamma\,|\widetilde{n+1}\rangle \tag{6.13}$$

We now have gathered what we need to look at the problem. We initialize the system in a the level that is not going to be periodically driven:

$$|\psi_i\rangle = \begin{bmatrix} 1 \\ 0 \\ \vdots \\ 0 \end{bmatrix} \tag{6.14}$$

Before the periodic driving, we have a simple linear level crossing, described by the Hamiltonian:

$$H = \begin{bmatrix} \epsilon(t) & \delta \\ \delta & E_1^{(n)} \end{bmatrix} \tag{6.15}$$

We have already looked at how a LZT looks like, we can describe the transition with the evolution operator N:

$$N\left|\psi_i\right\rangle_a = \begin{bmatrix} \sqrt{1-P_{LZ}}e^{-i\phi_s} & -\sqrt{P_{LZ}} \\ \sqrt{P_{LZ}} & \sqrt{1-P_{LZ}}e^{i\phi_s} \end{bmatrix} \begin{bmatrix} 1 \\ 0 \end{bmatrix} = \begin{bmatrix} \sqrt{1-P_{LZ}}e^{-i\phi_S} \\ \sqrt{P_{LZ}} \end{bmatrix} \tag{6.16}$$

From now on we will only write 4 of the components of the wave function, the ϵ, $E_1^{(n-1)}$, $E_1^{(n)}$ and $E_1^{(n+1)}$ components, where $E_x^{(y)}$ is the energy of the state in the y photon level in the x atom level, $|x,y\rangle$. After the transition we have:

$$|\psi_1\rangle = \begin{bmatrix} \sqrt{P_{LZ}} \\ 0 \\ \sqrt{1-P_{LZ}}e^{-i\phi_S} \\ 0 \end{bmatrix} = \begin{bmatrix} \beta \\ 0 \\ \zeta \\ 0 \end{bmatrix} \tag{6.17}$$

We now consider turning on the periodic driving. And introduce the Schrieffer-Wolff transformation, eq. (6.13):

$$|\widetilde{\psi_1}\rangle = \begin{bmatrix} \beta \\ -\gamma\zeta \\ \zeta \\ \gamma\zeta \end{bmatrix} \tag{6.18}$$

Finding the propagator from after the first crossing to the second crossing is simple since the Hamiltonian is now diagonal.

$$\widetilde{U}(t_1,t_2) = \begin{bmatrix} e^{-i\int_{t_1}^{t_2}\epsilon(t)dt} & 0 & 0 & 0 \\ 0 & e^{-iE_1^{(n-1)}T} & 0 & 0 \\ 0 & 0 & e^{-iE_1^{(n)}T} & 0 \\ 0 & 0 & 0 & e^{-iE_1^{(n+1)}T} \end{bmatrix} \tag{6.19}$$

Where $T = t_2 - t_1 = \tau + 2t^*$. The integral can be split into a τ dependent part and a phase that is not dependent on τ. $\int_{t_1}^{t_2}\epsilon(t)dt = \xi\tau + 2\int_{t_1}^{t_1+t^*}\epsilon(t) = \xi\tau + \phi_k$. For the sake of convenience we choose $E_1^{(n)} = 0$. This gives us the wave function right before the second crossing (t_2) in the transformed basis:

$$|\widetilde{\psi_2}\rangle = \begin{bmatrix} \beta e^{-i(\xi\tau-\phi_k)} \\ -\gamma\zeta e^{i(E_1T)} \\ \zeta \\ \gamma\zeta e^{-i(E_1T)} \end{bmatrix} \tag{6.20}$$

Where we have inserted $E_1^{(n-1)} = -E_1^{(n+1)}$. We now use eq. (6.12) to transform back to our original basis:

$$|\psi_2\rangle = \begin{bmatrix} \beta e^{-i(\xi\tau-\phi_k)} \\ \gamma\left(-\zeta e^{i(E_1T)} + \zeta\right) \\ \zeta \\ \gamma\left(\zeta e^{-i(E_1T)} - \zeta\right) \end{bmatrix} + \mathcal{O}(\gamma^2) = \begin{bmatrix} \bar{\beta} \\ \Gamma_1 \\ \Gamma_2 \\ \Gamma_3 \end{bmatrix} \tag{6.21}$$

At this point we have to take into account that we are working with coherent states, and so if we want to do a second level crossing we have to find the state in a photon number basis again. We can then simplify by writing this states as:

$$\widetilde{U}_{QM} \left|1, \alpha(0)\right\rangle = \zeta e^{-in\omega t} \sum_m B_m \left|1, n+m\right\rangle \tag{6.22}$$

where:

$$B_{-1} = -\gamma e^{i\omega t} + \gamma \tag{6.23}$$

$$B_0 = 1 \tag{6.24}$$

$$B_{-1} = \gamma e^{-i\omega t} - \gamma \tag{6.25}$$

We find the semi-classical time evolution of the level "1" tracing out the photon part:

$$\begin{aligned} \widetilde{U}_S \left|1\right\rangle &= \zeta \left\langle \alpha(t)|\widetilde{U}_{QM}|1, \alpha(0)\right\rangle \\ &= \zeta \left(\sum_k c_k^* e^{ik\omega t} \left\langle k\right| \right) \left(\sum_{m,n} c_n e^{-in\omega t} B_m \left|1, n+m\right\rangle \right) \\ &= \zeta \sum_{m,n} c_{n+m}^* c_n e^{im\omega t} B_m \left|1\right\rangle \end{aligned} \tag{6.26}$$

Since $c_{n+m} \approx c_n$ (intuitive since n is big and m is small, but it can also be shown using Stirling's approximation) we can use $\sum_n |c_n|^2 = 1$ to remove one of the sums and we get:

$$\begin{aligned} \widetilde{U}_S \left|1\right\rangle &= \zeta \sum_m e^{im\omega t} B_m \left|1\right\rangle \\ &= \zeta \left(e^{-i\omega t} B_{-1} + B_0 + e^{i\omega t} B_1 \right) \\ &= \zeta \left(\gamma(-1 + e^{-i\omega t}) + 1 + \gamma(1 - e^{i\omega t}) \right) \\ &= \zeta (1 + \gamma e^{-iE_1 t} - \gamma e^{iE_1 t}) \end{aligned} \tag{6.27}$$

We can then apply the LZT evolution matrix, N, which gives us the return amplitude A_{ret}

$$A_{ret} = -P_{LZ} e^{-i(\xi\tau + 2\phi_k)} + e^{-2i\phi_S}(1-P)(1 + \gamma e^{iE_1\tau} - \gamma e^{-iE_1\tau}) \tag{6.28}$$

Which when taken the absolute square gives us the return probability:

$$\begin{aligned} P_{ret} = P_{LZ}^2 &+ (1 - P_{LZ})^2 \\ &- 2P_{LZ}(1 - P_{LZ}) \cos(\xi\tau + 2\phi_k - 2\phi_S) \\ &- 2\gamma P_{LZ}(1 - P_{LZ}) \cos((\xi - E_1)\tau + 2\phi_k - 2\phi_S) \\ &+ 2\gamma P_{LZ}(1 - P_{LZ}) \cos((\xi + E_1)\tau + 2\phi_k - 2\phi_S) \end{aligned} \tag{6.29}$$

A result looking a lot like the case of the trapezoid magnetometer, interpreting it as paths, we have interference between the path that isn't oscillating and the three photon levels, the one that is crossed and its two neighbours. When the driving is turned on, the state leaks into the sidebands close to it, and we see effects of this in the interference in this experiment. This is exactly what we see in simulations, figure 6.3. In this graph the Fourier transform of the return probability as a function of wait time, τ, is taken to clearly show that we have the three periodic functions in eq. (6.29), two of the peaks dampened with $\gamma = 4/33$. Showing how much the state leaks out into its sidebands. We also see hints of the higher order results we discarded.

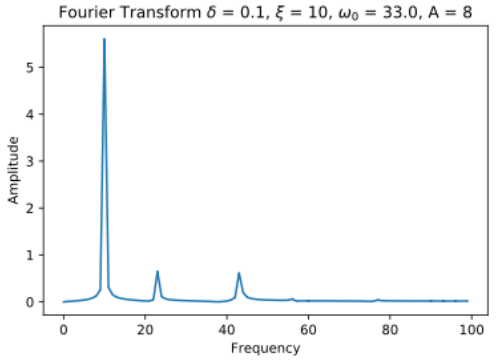

Figure 6.3: Fourier transform of the return probability as a function of the length of the driving, τ

6.4.2 Number state LZT

From the Hamiltonian:

$$H = (\omega_0 - vt)\left|0\right\rangle\left\langle 0\right| + \omega a^\dagger a - A\left|1\right\rangle\left\langle 1\right|(a + a^\dagger) - \delta(\left|0\right\rangle\left\langle 1\right| + \left|1\right\rangle\left\langle 0\right|), \tag{6.30}$$

We can see that there is coupling between the two levels, with a coupling strength, δ. If we don't look to careful we might expect there to be only one LZT in a sweep, that is when all the photon bands cross with their corresponding counterpart in the other level. Assuming A is small compared to the ω this is going to be the biggest contributor to state transfer, but it isn't the only one. All the photon sidebands of the 1 level are coupled to the one above and below itself as we can see from the truncated effective Hamiltonian at time $t = 0$:

$$H = \begin{bmatrix} \omega_0 & 0 & 0 & & \delta & & & \\ 0 & \omega_0 + \omega & 0 & & & \delta & & \\ 0 & 0 & \omega_0 + 2\omega & & & & \delta & \\ & & & \ddots & & & & \\ \delta & & & & 0 & A & 0 & \\ & \delta & & & A & \omega & A\sqrt{2} & \\ & & \delta & & 0 & A\sqrt{2} & 2\omega & \\ & & & & & & & \ddots \end{bmatrix} \tag{6.31}$$

Every photon level of the $|0\rangle$ state is indirectly coupled to all photon levels in the $|1\rangle$ state. We can demonstrate this by initializing the system in the $|0, 0\rangle$ state with $\omega_0 = 2.5\omega$ and letting it propagate for a time $5\omega/v$, with a large coupling A. The instantaneous level structure (with exaggerated coupling) is shown in figure 6.5. In figure 6.4 we look at the probability of the system being in the $|1\rangle$ state during the process described, meaning that it has transferred. We can see 5 points of population transfer, corresponding to the 5 level/sideband crossings. The big jump in the middle is when the 0 photon levels of the atom states crosses. The effects of the crossings before and after this get smaller and smaller as we expect.

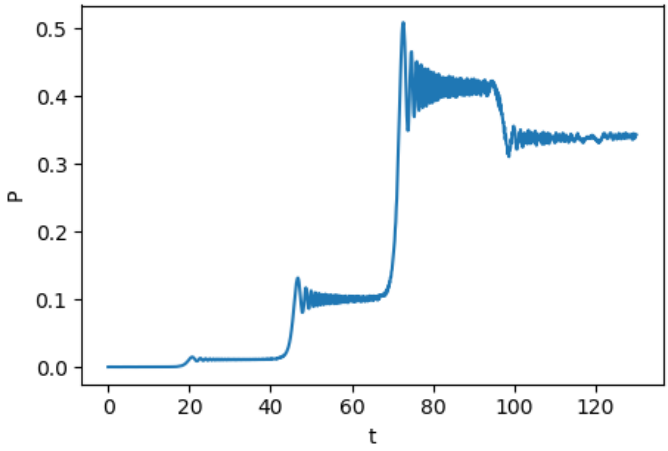

Figure 6.4: The probability of transfer from the 0 state (P) in an example of a sweep of the 0 level, where the system is initialized in the $|0,0\rangle$ state and is being driven for a time, $5\omega/v$. There are 5 steps, 4 of which are easy to see, that corresponds to level crossings. A=12, v=1, $\delta = 0.3$, $\omega = 26$, $\omega_0 = 2.5 * w$

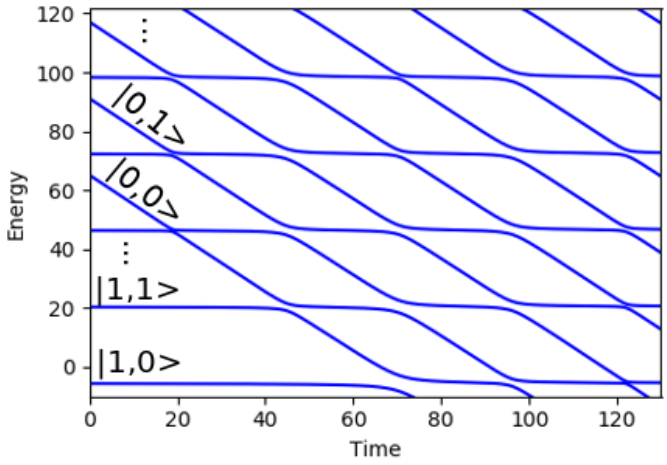

Figure 6.5: Instantaneous energy levels with exaggerated couplings of a LZ sweep with a TLS coupled to a bosonic mode

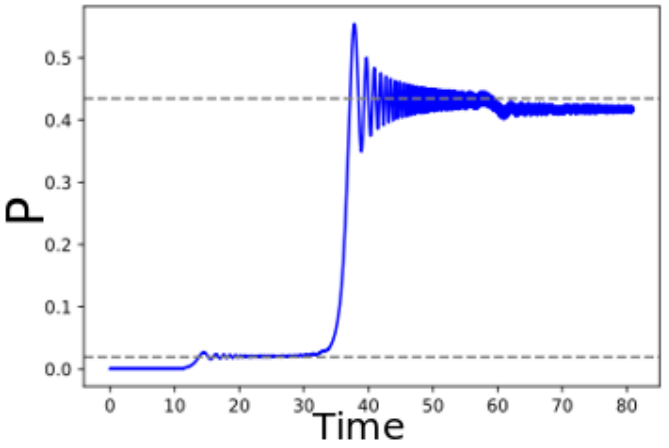

Figure 6.6: Simulation of three LZT, first and last being sidebands crossing with 0 photon levels. The plot is of the probability of the system staying in the "0" atom state. The lower grey dotted line is the analytic prediction using the LZ formula with the effective coupling δ' from eq. (6.32) and the upper grey line is the predicted probability after two crossings from (6.33). A=5 , v=1, $\delta = 0.3$, $\omega = 26$, $\omega_0 = 1.5\omega$

6.4.3 Example of three crossings

We take a step back and look a more specific example where we encounter three LZT. We initialize the system in the $|0, 0\rangle$ state between the first and second sidebands of the lower level, $\omega_0 = 1.5\omega$, and drive it down $3\omega/v$, i.e. through three avoided level crossings. Time dependent instantaneous energy spectrum of the procedure is shown in figure 6.8. This example will touch on the three main parts that makes this particular system interesting: indirect coupling, consecutive crossings and interference effects. Let's first have a look at the first crossing. The upper level is not directly coupled to the sideband but it is indirectly coupled via the 0 photon state of the lower level, which is coupled to the first sideband as we can see in eq. (6.31). If the couplings are weak compared to the photon energy, ω, we can find the effective coupling with perturbation theory. One way is to use the Schrieffer Wolff transformation introduced in section 4.2 and appendix A. We here saw that a two levels crossing with each other, where both had coupling elements to a third state, had the effective coupling of the two coupling elements multiplied and divided by the distance to the third level. The coupling between the "0" state with n photons and the "1" state $n + 1$ a photon is then:

$$\langle 0, n| H |1, n + 1\rangle = \frac{\sqrt{n + 1}A\delta}{\omega} \tag{6.32}$$

We see the similarity with the longitudinal driving of the energy levels. In that case the sidebands had suppression factor $J_1(A/\omega)$ which is linear for small A/ω. The other sidebands are also similar but we will come back to this. For the second crossing in figure 6.6 we need to consider that there has been some transfer already. We can think about it in the way of paths like we did in the case of the trapezoid magnetometer, there are two paths that lead to transfer. Transfer at the first crossing and not transfer at the other, and then there is the path of no transfer

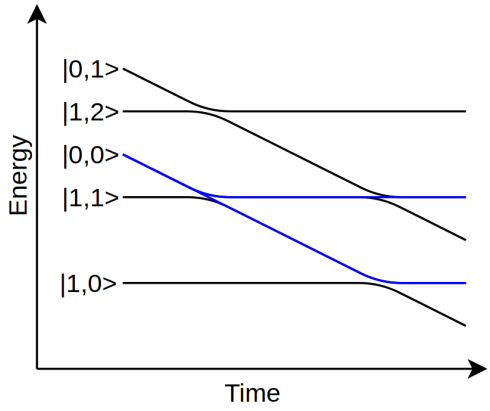

Figure 6.7: Energy spectrum of a LZ sweep described in section 6.4.3, showing the paths that leads to transfer from one atom state to another after two crossings, starting in the $|0,0\rangle$ state

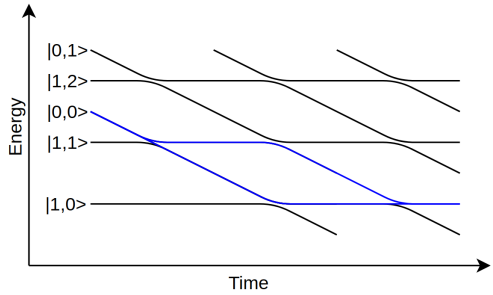

Figure 6.8: Energy spectrum of a LZ sweep described in section 6.4.3, showing the two paths interfere after three crossings in blue, starting in the $|0,0\rangle$ state

in the first crossing and crossing in the second crossing, the two paths are shown as blue lines in figure 6.7. The full transfer probability is then:

$$P_t = (1 - P_{LZ}^{'})P_{LZ} + P_{LZ}^{'}(1 - P_{LZ}) \tag{6.33}$$

Where the primed Landau Zener probability is defined with the effective coupling $\langle 0, n| H |1, n+1\rangle$ instead of δ. And as we can see from figure 6.6 this analytical result fits well with the example in the simulation. As mentioned earlier the third crossing is more complicated due to interference. The interference we talk about is between the path that transfer at the first crossing and the one that does not, both following the adiabatic energy level at the second crossing and then ending up in the same level in the end, paths shown as blue lines in figure 6.8. The difference in phase between these paths is the area between the two paths in the energy-time diagram of figure 6.5, i.e. one of the smooth corner rhombus shapes we see in the figure. This area can be estimated by a rhombus and have the area $A = \omega^2/v$. If we want the full picture of the interference we also have to account for the Stokes phase. We will not go into this now, but

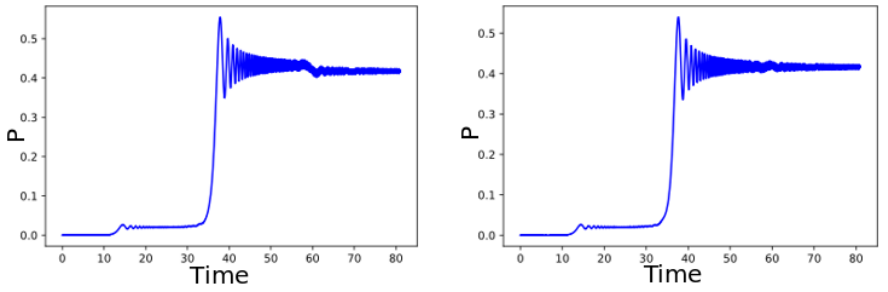

Figure 6.9: Shifting the rhombus area in figure 6.5 by an odd number of π (in this case making $\omega = 27$ in the right plot) makes makes the interference go from constructive to destructive in the last crossing, making it disappear with the right choice in driving speed. A=5 , v=1, $\delta = 0.3$, $\omega = 26$, $\omega_0 = 1.5\omega$ for the left plot

keep this in mind as we will look at this later. If we start out with a system that shows full constructive interference we can tune either of the variables ω or v so that the area is shifted by π, the system will then go from full constructive interference to full destructive interference, we can see this shift in figure 6.9. This is something we didn't see in the transverse case, as two crossing is not enough to make interference (at least with a single number state). Interference gives us another way of manipulating the system and is something we will look into in the next chapter, where we are going to discuss possible use cases.

6.4.4 Effective coupling

We want to find the effective coupling between $|0, n\rangle$ and $|1, m\rangle$, $\langle 0, n| H |1, m\rangle$. If $n = m$ then the coupling is just δ, and we have looked at the case $|m - n| = 1$ above. We are going to look at the case where $m >= n$, but for $n > m$ it should just be to switch n and m due to symmetry. To do this we will use a sort of induction, where we use the known indirect couplings to find more indirect couplings. Generally what we are going to have a look at is Hamiltonians (or Hamiltonians containing subsystems) of the type:

$$H_e x = \begin{bmatrix} a & 0 & \delta_1 \\ 0 & b & \delta_2 \\ \delta_1 & \delta_2 & c \end{bmatrix} \tag{6.34}$$

Where two levels upper levels are indirectly coupled by a third level. We assume that this is the only indirect connection. We are going to use Schrieffer Wolff to block diagonalize and find the coupling between level a and b. The first order correction to the a-b subsystem is going to be:

$$\frac{1}{2}[S_1, V]_{11} = \frac{V_{12}V_{21}}{E} = \begin{bmatrix} \frac{\delta_1^2}{(a-c)} & \frac{\delta_1\delta_2}{2}\left(\frac{1}{a-c} + \frac{1}{b-c}\right) \\ \frac{\delta_1\delta_2}{2}\left(\frac{1}{a-c} + \frac{1}{b-c}\right) & \frac{\delta_1^2}{(b-c)} \end{bmatrix} \tag{6.35}$$

As we can see the diagonal elements shift the energy, and thereby when the crossing happens, but we are not concerned with this here. To remind our selves, we are working with the Hamil-

tonian:

$$H = (\omega_0 - vt)\left|0\right\rangle\left\langle 0\right| + \omega a^\dagger a - A\left|1\right\rangle\left\langle 1\right|(a + a^\dagger) - \delta(\left|0\right\rangle\left\langle 1\right| + \left|1\right\rangle\left\langle 0\right|) \tag{6.36}$$

The two n photon levels of the 0 and 1 subsystems are always going to be connected by the coupling element $\langle 0, n| H |1, n\rangle = \delta$. We are going to use this coupling as a first indirect coupling, and find the effective coupling between the levels in the 1 subsystem. Specifically we are trying to find $\langle 0, n| H |1, m\rangle$, when the levels cross, and we are going to use the two matrix elements $\langle 0, n| H |1, n\rangle = \delta$ and $\langle 1, n| H |1, m\rangle$ to do so.

$$\begin{aligned}\langle 0, n| H |1, m\rangle &\approx \frac{1}{2}\langle 0, n| H |1, n\rangle\langle 1, n| H |1, m\rangle\left(\frac{1}{E_0^{(n)} - E_1^{(n)}} + \frac{1}{E_1^{(m)} - E_1^{(n)}}\right) \\ &= \langle 0, n| H |1, n\rangle\langle 1, n| H |1, m\rangle\frac{1}{(m-n)\omega}\end{aligned} \tag{6.37}$$

$\langle 1, n| H |1, m\rangle$ is therefore what we need to find. We start by looking at $\langle 1, n| H |1, n+2\rangle$, and we know that $\langle 1, n| H |1, n+1\rangle = \sqrt{n+1}A$ and that $\langle 1, n+1| H |1, n+2\rangle = \sqrt{n+2}A$, so we use Schrieffer-Wolff again to find:

$$\begin{aligned}\langle 1, n| H |1, n+2\rangle &\approx \frac{1}{2}\langle 1, n| H |1, n+1\rangle\langle 1, n+1| H |1, n+2\rangle \\ &\times\left(\frac{1}{E_1^{(n)} - E_1^{(n+1)}} + \frac{1}{E_1^{(n+1)} - E_1^{(n+2)}}\right) \\ &= -\frac{\sqrt{n+1}\sqrt{n+2}A^2}{\omega}\end{aligned} \tag{6.38}$$

We can then use this to find the indirect coupling between $|1, n\rangle$ and $|1, n+3\rangle$, and so on. Each new term m' is going to multiply the previous with $A\sqrt{n+m'}$ and divide by $-(m'-1)\omega$. This recurrence relation gives us the expression for the effective couplings between the photon states in the "1" level. The general effective coupling is then going to be:

$$\langle 1, n| H |1, m\rangle \approx (-1)^{(m-n-1)}\sqrt{\frac{m!}{n!}}\frac{1}{(m-n-1)!}\frac{A^{(m-n)}}{\omega^{(m-n-1)}} \tag{6.39}$$

We can then find the full effective coupling we wanted to find:

$$\langle 0, n| H |1, m\rangle \approx (-1)^{(m-n-1)}\delta\sqrt{\frac{m!}{n!}}\frac{1}{(m-n)!}\left(\frac{A}{\omega}\right)^{(m-n)} \tag{6.40}$$

Chapter 7

Application: Manipulation and creation of superpositions of coherent photon states

In the previous chapters we have discussed how a TLS coupled to a bosonic mode behaves, in this chapter we will focus on how these level crossings can manipulate photon states in specific ways. We are going to keep to the longitudinal case and the photon states are going to be the cat states that we have mentioned. Having qubits that are made up of photons states seems promising [41], but if they are going to be useful in quantum information processing, we need to be able to manipulate them, and more importantly, make them. First we will look at turning the different cat states into other cat states using adiabatic transfer and interference. After that we will propose a method of creating cat states using some of the properties of the photon-assisted Landau-Zener transition that we have discussed up til now.

7.1 Even to odd coherent states

One simple case of coherent state manipulation by LZT is to turn an even coherent superposition state into an odd, or the other way around. This is called a bit flip, and is one of the operations needed to make a quantum computer. As a reminder we are working with the Hamiltonian:

$$H = (\omega_0 - vt)\left|0\right\rangle\left\langle 0\right| + \omega a^\dagger a - A\left|1\right\rangle\left\langle 1\right|(a + a^\dagger) - \delta(\left|0\right\rangle\left\langle 1\right| + \left|1\right\rangle\left\langle 0\right|) \tag{7.1}$$

The effective coupling we are going to work with is:

$$\left\langle 0, n\right| H \left|1, m\right\rangle \approx (-1)^{(m-n-1)}\delta\sqrt{\frac{m!}{n!}}\frac{1}{(m-n)!}\left(\frac{A}{\omega}\right)^{(m-n)} \tag{7.2}$$

This can be done by initializing the photon field in the state that we want to flip, with the atom levels less than the energy of a photon apart. Then driving the levels through through at

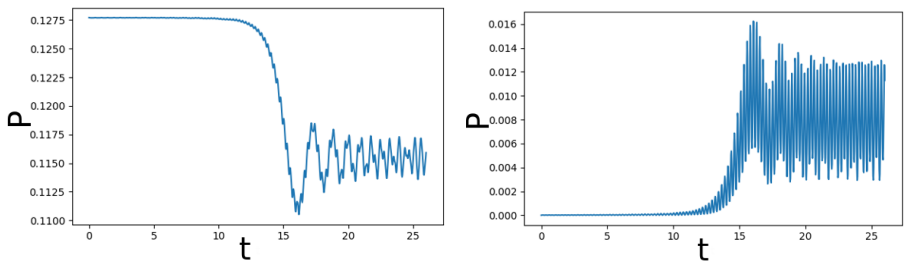

(a) (b)

Figure 7.1: Showing the difference in how number state populations evolve in the "0" and "1" state. P being the probability of being in the 5 photon state. Level "0" to the left, and level "1" to the right. $\alpha^2 = 7$, A=5, v=1, $\delta = 0.3$, $\omega = 26$, $\omega_0 = 1.5\omega$

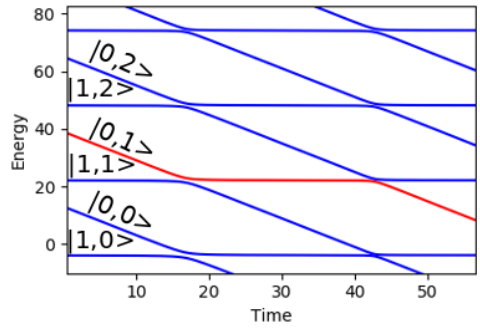

Figure 7.2: The red adiabatic level being an example of odd being connected to even

least two crossings. This with a "slow enough" driving speed, and then projecting to the "0" level when done. The reason the driving needs to be slow is that the system then follows the adiabatic states, which takes number states from n to n+1 in two crossings, as seen an example of in figure 7.2. What is meant by projection is that we only look at the photons associated with one of the levels. In experiments the way you do this is to measure whether the system is in the "0" or the "1" level, collapsing this part of the wave function. The reason we do this projection is twofold, first the photon state of the "1" level is going to be less well behaved then the "0" level due to the coupling between energy levels. We can see this in 7.1, where we have done a photon assisted Landau-Zener transition, and we are looking at the probability of being in the $|0, 5\rangle$ and the $|1, 5\rangle$ state side by side. The second reason is that the full photon distribution is more complicated, as this is a superposition of the two photon states of the atom levels. So for simplicity and clarity we just look at the "0" level photons. The state we end up with is a superposition of number states that is similar to what we started with, but the coefficients are now $c_n \to c_{n-1}$. The reason we don't necessarily need to stop after two crossings is that the crossings have a weaker and weaker effective coupling. We can make it so that the second crossing is substantial, but the third (and later) are insignificant.

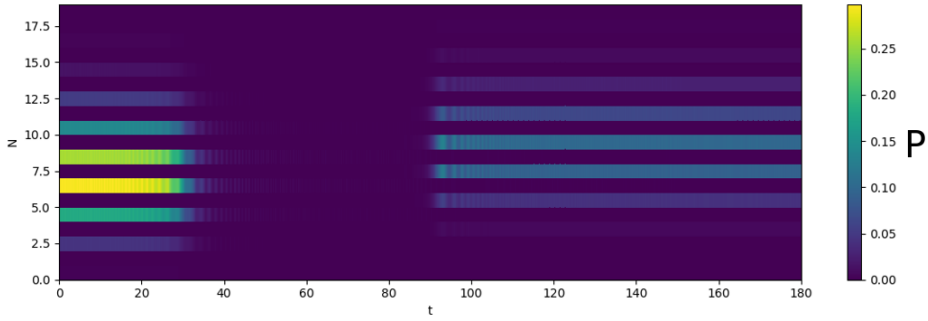

Figure 7.3: The photon distribution of the "0" level, starting with an even coherent superposition turning to a state after two crossings. $\alpha^2 = 7$, A=2, v=0.5, δ=1, ω=30, $\omega_0 = 0.5\omega$

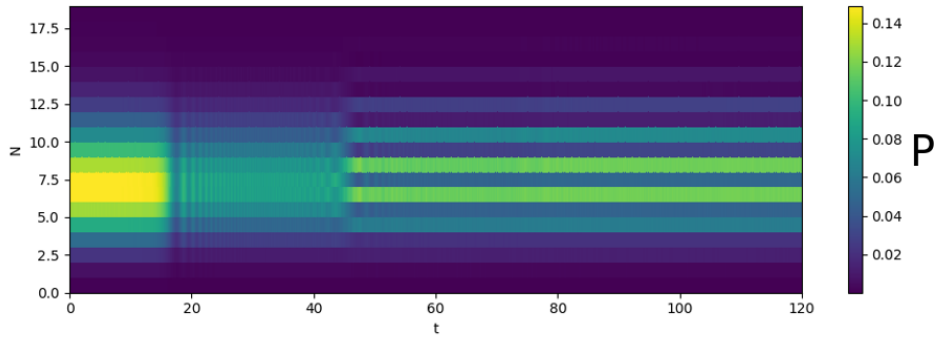

Figure 7.4: sweep turning YS to even after two crossings, $\alpha^2 = 7$, A=4, v=1, $\delta = \sqrt{\ln(0.5)v/(-2\pi)}$, $\omega = 30$, $\omega_0 = 0.5 * \omega$

7.2 Yurke-Stoler to even/odd coherent state

We found in previous chapters that we can get interference effects when we initialize the system in a photon number state and run the system through at least three level crossings. When working with superpositions of coherent states it is a bit more complicated. While the number states that make up a coherent state start out with the same phase, the number states that make up a superposition of two coherent states does not necessarily. There is therefore another phase to keep track of, but as we will see this phase enables us to do new things.

We look at what will happen if we initialize the system in the "0" atom level with a YS photon state, starting with $\omega_0 = 1.5\omega$ and driving the system through four crossings. As a reminder the state we are going to initialize in is on the form:

$$|\psi\rangle = |\alpha\rangle + i\,|-\alpha\rangle \tag{7.3}$$

In figure 7.4 we see that something quite interesting happens to the photon state after just two crossings. The superposition has changed from a YS to an even state. That the event happened

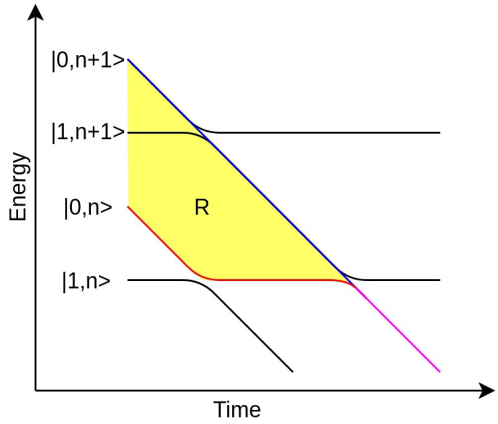

Figure 7.5: A section of the level structure showing the two paths (red and blue) interfering when turning a YS state into an even or an odd state. The area/phase referred to as R is shown in yellow

after just two crossings tells us that it is not caused by interference of a single number state with itself, but has to be interference between "neighboring" number states.

To analyse this we first have a look at the Yurke-Stoler state. It is a superposition of two coherent states, in terms of number states it can be written as:

$$\begin{aligned} |\alpha\rangle &= e^{-\frac{|\alpha|^2}{2}} \sum_{n=0}^{\infty} \frac{\alpha^n}{\sqrt{n!}} |n\rangle + ie^{-\frac{|\alpha|^2}{2}} \sum_{n=0}^{\infty} \frac{(-\alpha)^n}{\sqrt{n!}} |n\rangle \\ &= \sum_{n=0}^{\infty} c_n + i(-1)^n c_n |n\rangle = \sum_{n=0}^{\infty} b_n |n\rangle \end{aligned} \tag{7.4}$$

Where c_n are the real coefficients for the coherent state $|\alpha\rangle$. The two coefficients b_n and b_{n+1} are $\frac{\pi}{2}$ out of phase:

$$b_n = (c_n + ic_n)/N, \quad \text{n is even} \tag{7.5}$$

$$b_n = (c_n - ic_n)/N, \quad \text{n is odd} \tag{7.6}$$

We look at the interference between two number states in the YS state. That is the path starting in $|0, n+1\rangle$ then transferring at the two transitions and the path starting in $|0, n\rangle$ not transferring twice, both ending up in $|0, n+1\rangle$ level. The paths that interfere are marked with blue and red respectively in figure 7.5. We will assume that the coefficient of each of these number states have the same modulus, something that will be approximately true for coefficients close to the expectation value. There are three different phases to keep track of. The phase that the state start out with ($|0, n\rangle$ and $|0, n+1\rangle$ having a phase $pi/2$ in difference because we have a YS state), the acquired phase $e^{-i\int E_{r,b}dt}$, where $E_{r,b}$ are the energies shown as red and blue paths in figure 7.5. Lastly the Stokes phase that comes from transfer from one diabatic level to another.

The first path (blue) acquires no Stokes phase, the second path (red) acquires two different Stokes phases with opposite signs. The Stokes phases are generally not the same since the two

adiabatic crossings have different coupling strengths, so that path acquires a phase $\phi'_S - \phi_S$. Then there is the difference in dynamically acquired phase, the area between the red and blue line, which we will denote by R, seen in yellow in figure 7.5. The difference in phase, given that n is odd, between the two paths is then:

$$\phi^{(1)}_{diff} = (\pi/2 + R) - (\phi'_S - \phi_S) \tag{7.7}$$

The primed Stoke phase is the one with the effective coupling $\delta_{n,n+1}$. And what is interesting is that when n is even instead of odd the expression above turns to:

$$\phi^{(2)}_{diff} = R - (\phi'_S - \phi_S + \pi/2) \tag{7.8}$$

A shift of π, meaning that when $\phi^{(1)}_{diff} = 2m\pi$ we get constructive interference in the $|0, n+1\rangle$ state while we get destructive interference in $|0, n+2\rangle$ and $|0, n\rangle$. Explaining why we get the alternating interference pattern we found. It also gives us an expression for the phase R required to make even and odd states:

$$R = m\pi + \pi/2 + (\phi'_S - \phi_S), \quad m \in \mathbb{Z} \tag{7.9}$$

If we have a constant sweep speed, v, the phase R can be estimated by the a trapezoid in the energy-time diagram, in terms of frequency of the photon mode and the sweeping speed it is given by:

$$R = \frac{\omega^2}{v} \tag{7.10}$$

We see then that we can tune the driving speed or the frequency so that we get interference. The difference in Stokes phases, $\phi'_S - \phi_S$, is dependent on the driving speed and frequency as well (in fairly complicate way), so finding a set of parameters might difficult analytically without setting any initial conditions. We can however use that the Stokes phase is a function of A/ω in the case of ϕ'_S, and they are both a function of δ^2/v. By setting these ratios we can calculate the difference in Stokes phases easily and then tune either v or ω to get the interference we want, then adjust δ or A so that the ratios are what we decided in the beginning. Another way of manipulating the area that avoids the ω and v dependence of the Stokes phases, is to manipulate the phase, R, by pausing the sweep between the crossings, but this might be more difficult to implement experimentally

7.3 Producing cat states using Landau Zener Transitions

While we have looked into how to manipulate the cat states, it would also be very useful to be able to make them. As stated these cat states have a wide variety of use cases, but producing them is difficult, especially big cat states [49, 50]. What we are proposing in this section is a way of utilizing the properties of the photon assisted LZT, in a fairly simple method using a sweeping level that changes speed once, to make these cat states. We are going to be using the photon number dependence of the avoided level crossing, which we can see from the effective coupling element:

$$\langle 0, n| H |1, m\rangle \approx (-1)^{m-n-1}\delta\sqrt{\frac{m!}{n!}}\frac{1}{(m-n)!}\left(\frac{A}{\omega}\right)^{(m-n)} \tag{7.11}$$

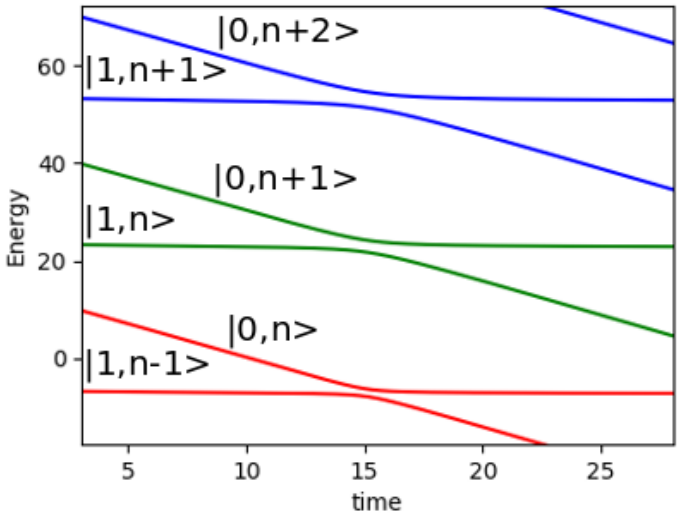

Figure 7.6: We see that the avoided crossing is stronger the higher the photon number is, the blue crossing being more avoided than the red.

Comparing two coupling elements where m-n are the same:

$$\frac{\langle 0,n|\, H\, |1,m\rangle}{\langle 0,n+1|\, H\, |1,m+1\rangle} = \frac{\sqrt{\frac{m!}{n!}}}{\sqrt{\frac{(m+1)!}{(n+1)!}}} = \frac{n+1}{m+1} \tag{7.12}$$

Since we have defined $m \geq n$ we see that higher photon number means higher coupling, and therefore stronger anti crossings, except when $n = m$. In figure 7.6 we see that the blue crossing has a stronger anti crossing than the green and so on. Up til now we have approximated the dynamic phases by calculating simple geometric shapes instead of integrating the adiabatic energy levels. If the coupling is strong or the driving speed is slow, this is no longer a good approximation.

The procedure we propose is described in figure 7.7. The system is initialized in the 0 level with the photon field in a coherent state. We start by crossing the $|0,n\rangle$ with $|1,n\rangle$ level at a sweep speed such that we split the state 50/50 in the two atom levels (the crossing just before t_1). Then we slow the sweep speed down, so that the next crossing is adiabatic, even though the coupling is much weaker. For this example we will use the coincidence that the slow down needed to have the desired effect in the crossing at $t = 0$ is roughly the same slowdown needed to make the crossing at $t = t_2$ close to 50/50. It would of course be better to change the speed again, so that this crossing is as desired, but since this crossing is just for recombination and we are trying to show a concept, this will do.

We will treat the number states that make up the cat state separately, and so we start by looking at the $|0,n\rangle$ number state. In figure 7.7, we see that it splits at the crossing before t_1

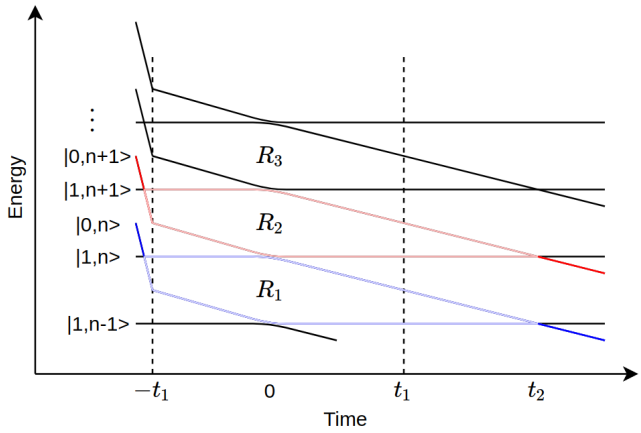

Figure 7.7: The procedure we suggest for making cat states

and then travels along the two blue paths before being recombined at t_2, where the two paths can interfere. We look at the paths ending up in the 0 state. How they interfere depends on the phases they acquire. They are going to acquire a geometric phase ϕ_g, which is close to the same for all number states. The geometric phase acquired at the first crossing is exactly the same for all photon number state. For the second crossing, it is approximately the same because Stokes phase is 0 in the adiabatic limit. For the third crossing it is also approximately the same because we have defined the crossing to be 50/50. The dynamically acquired phase on the other hand is not the same for all number states. The difference of this dynamical phase for the two paths, ϕ_b, is recognised in figure 7.7 as the area encapsulated by the blue lines. This area is mainly dependent on the frequency of the mode and the sweep speed, but remember that the avoided level crossing at $t = 0$ is dependent on n, as we saw in 7.6, so this part of the phase is dependent on what photon level we are looking at. This crossing is therefore what we are going to use to make the cat states.

Say that the parameters are such that the blue paths end up interfering constructively. We can then imagine, if the parameters are just right, that the red paths interfere destructively. This being because the dynamical phase difference, ϕ_r, encapsulated by the red lines in 7.7, is π smaller than ϕ_b due to having stronger anti crossings. This alternating behaviour of constructive and destructive interference would then make an even or an odd state, depending on whether n is even or odd .

The interference problem can be split in two tasks, one is to ensure that the difference $\phi_b - \phi_r$ is π and the other is to make sure that the blue path interferes fully constructively or destructively. We will however concentrate on the first problem, as we have already discussed the second part.

7.3.1 Calculating the slowdown speed required to make cat states

In this section we are going to find an estimate for the phase difference between the red and the blue area, $\phi_b - \phi_r = \phi_t$, in figure 7.7. We are going to look at the problem in three parts.

First there is the region $t < -t_1$, this crossing is the same for all photon levels as we can see this from eq. (7.11) with n = m. So any contribution to ϕ_b is going to be close to the same as one in ϕ_r. The contribution to the phase difference, ϕ_t can therefore approximated to zero. Then there is the main part in the middle, where $-t_1 < t < t_1$, In this crossing the adiabacity parameter is high and the coupling is photon number dependent. The phase difference gained in this region, $R_1 - R_2$, is going to be the main focus of this section. The last region $t_1 < t$ also has avoided level crossings that is photon number dependent, but the effective couplings here are weak. The difference between photon numbers are therefore small, and so we neglect it as a first approximation using the same argument as the first region. $R_1 - R_2$ is therefore the main contributor to the total phase difference, $\phi_t \approx R_1 - R_2$. We start by looking at R_1:

$$R_1 = \int_{-t_1}^{t_1} \left(\frac{-vt - \sqrt{(vt)^2 + 4\delta_n^2}}{2} + \omega \right) dt - \int_{-t_1}^{t_1} \left(\frac{-vt + \sqrt{(vt)^2 + 4\delta_{n+1}^2}}{2} \right) dt \quad (7.13)$$

$$= 2\omega t_1 - \frac{1}{2} \int_{-t_1}^{t_1} \left(\sqrt{(vt)^2 + 4\delta_n^2} + \sqrt{(vt)^2 + 4\delta_{n+1}^2} \right) dt \quad (7.14)$$

Where the integration limits are shown in figure 7.7, and the couplings δ_x are defined as:

$$\delta_n = \langle 0, n-1 | \, H \, | 0, n \rangle = \delta \sqrt{n} \left(\frac{A}{\omega} \right) \quad (7.15)$$

We focus on the first term in the integration:

$$\int_{-t_1}^{t_1} \sqrt{(vt)^2 + 4\delta_n^2} dt = t_1 \sqrt{(vt_1)^2 + 4\delta_n^2} + \frac{4\delta_n^2 \tanh^{-1} \left(\frac{vt_1}{\sqrt{(vt_1)^2 + 4\delta_n^2}} \right)}{v} \quad (7.16)$$

Similarly for the second term:

$$\int_{-t_1}^{t_1} \sqrt{(vt)^2 + 4\delta_{n+1}^2} dt = t_1 \sqrt{(vt_1)^2 + 4\delta_{n+1}^2} + \frac{4\delta_{n+1}^2 \tanh^{-1} \left(\frac{vt_1}{\sqrt{(vt_1)^2 + 4\delta_{n+1}^2}} \right)}{v} \quad (7.17)$$

The area R_2 can be calculated letting $n \to n+1$ in the calculation above. We insert $t_1 = \omega/(2v)$, the phase difference becomes:

$$\begin{aligned}
R_1 - R_2 &= \frac{(\omega/2)}{2v}\left(-\sqrt{(\omega/2)^2+4\delta_n^2}+\sqrt{(\omega/2)^2+4\delta_{n+2}^2}\right) \\
&+ \frac{1}{2v}\left(-4\delta_n^2\tanh^{-1}\left(\frac{(\omega/2)}{\sqrt{(\omega/2)^2+4\delta_n^2}}\right)+4\delta_{n+2}^2\tanh^{-1}\left(\frac{(\omega/2)}{\sqrt{(\omega/2)^2+4\delta_{n+2}^2}}\right)\right) \\
&\approx -\frac{1}{8v}\left(4\delta_n^2-4\delta_{n+2}^2\right) \\
&- \frac{1}{2v}\left(4\delta_n^2\tanh^{-1}\left(\frac{(\omega/2)}{\sqrt{(\omega/2)^2+4\delta_n^2}}\right)-4\delta_{n+2}^2\tanh^{-1}\left(\frac{(\omega/2)}{\sqrt{(\omega/2)^2+4\delta_{n+2}^2}}\right)\right) \\
&= \frac{2\delta^2}{v}\left(\frac{A}{\omega}\right)^2\left[-n\tanh^{-1}\left(\frac{(\omega/2)}{\sqrt{(\omega/2)^2+4\delta_n^2}}\right)\right. \\
&\qquad \left.+(n+2)\tanh^{-1}\left(\frac{(\omega/2)}{\sqrt{(\omega/2)^2+4\delta_{n+2}^2}}\right)-\frac{1}{2}\right]
\end{aligned} \tag{7.18}$$

We can simplify the two $\tanh^{-1}$ functions, by expanding in small couplings, δ_n:

$$\tanh^{-1}\left(\frac{(\omega/2)}{\sqrt{(\omega/2)^2+4\delta_n^2}}\right) \approx -\frac{1}{2}\ln\left(\frac{4\delta_n^2}{\omega^2}\right) \tag{7.19}$$

Giving us simplified expression for $R_1 - R_2$:

$$R_1 - R_2 = \frac{1}{v}\left(\frac{A\delta}{\omega}\right)^2\left(1+n\ln\left(\frac{2+n}{n}\right)+2\ln\left(\frac{4(2+n)(\delta A)^2}{\omega^4}\right)\right) \tag{7.20}$$

The phase difference, is as we can see n dependent. For large n however, this dependence is weak. Bigger coherent states are therefore better with this method, contrary to other methods of creating cat states. The condition for making cat states on the form we have looked at is:

$$R_1 - R_2 = (2m+1)\pi, \quad m \in \mathcal{Z} \tag{7.21}$$

We can see the effect of the procedure on the "0" atom state photon field in figures 7.8 and 7.9 for a relatively small cat state, $\alpha^2 = 7$, chosen because of computation limitations. We can see some smearing of the two coherent states in the Wigner plot, which we expect due to the n dependence of the phase difference. Doing the calculation for the parameters of the simulation shown in 7.8 and 7.9 using eq. (7.18) we get the phase difference $\phi \approx 1.13\pi$, for $n = 7$. A bit higher than what is the resonance condition, but this as we expect. The phase difference we calculated in (7.18), and hence (7.20), over estimates the phase difference. The last crossing (the one a t_2) affects the phase difference, but with the opposite sign. At first sight this might seem insignificant, but while the coupling is much smaller than the previous crossings at $t = 0$,

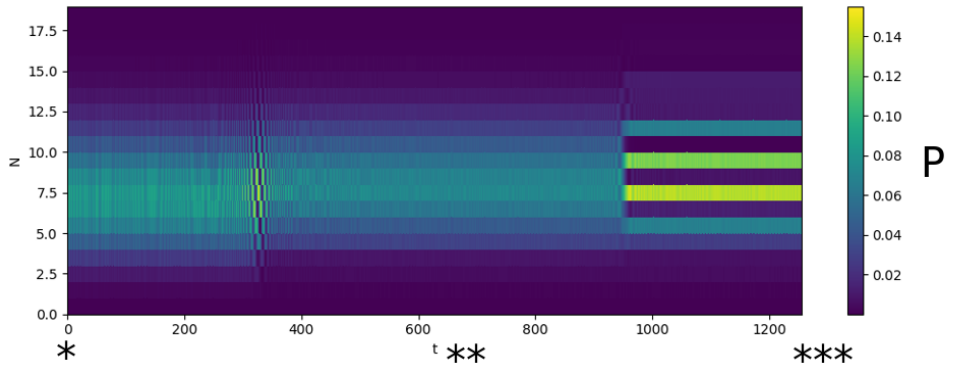

Figure 7.8: Photon state of the $|0\rangle$ state, during the process described to make cat states, $\alpha^2 = 7$, A=4, v=6, $\delta = \sqrt{\ln(0.5)v/(-2\pi)}\,\omega = 30$, $\omega_0 = 0.5 * \omega$, slowDown=125

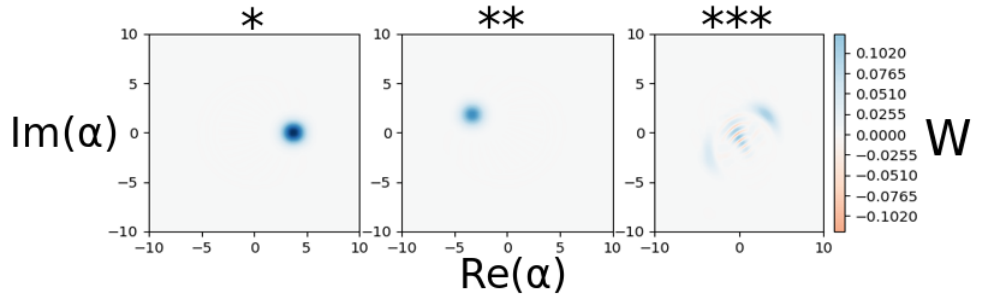

Figure 7.9: Wigner plot of the production of cat states by having a adiabatic level crossing, the time of the plots are marked with corresponding asterisks in figure 7.8, all of the after projection to the $|0\rangle$ state. $\alpha^2 = 7$, A=4, v=6, $\delta = \sqrt{\ln(0.5)v/(-2\pi)}\,\omega = 30$, $\omega_0 = 0.5\omega$, slowDown=125

it is also much more dependent on the photon number. It is still small but what we can do if we want to find error correction is to do the calculation above but substituting in the effective couplings of the crossings at t_2. The effective couplings for these crossings are:

$$\delta_n = \langle 0, n-1|\, H\, |0, n+1\rangle = \delta\sqrt{n}\sqrt{(n+1)}\left(\frac{A}{\omega}\right)^2 \tag{7.22}$$

Not only are we able to make the cat states on the form of eq. (5.20), we can in general make cat states with whatever phase between the amplitudes of the two macroscopic states we want by tuning $R_1 - R_2$. We could conceivably make an even more complicated superposition. E.x. a superposition of four coherent states with amplitudes $\pi/2$ out of phase. We could do this by doing the procedure above again with a cat state instead of a coherent state, and a phase shift of $\pi/2$ instead of π

Chapter 8

Concluding remarks

IIn this thesis we investigate photon-assisted Landau-Zener transitions in driven few-level systems. We both treat the driving field semi-classically (as a time-dependent parameter in the Hamiltonian) and fully quantum-mechanically (as a photon field). We start by introducing the basic ingredients: Looking at the well known Landau-Zener problem, and show a simple method for deriving the famous Landau-Zener formula, then having a look at what happens when you drive the energy levels periodically. Both in the case of weak driving, where we saw the emergence of photon sidebands and Rabi oscillations, and in the case of strong driving where we briefly looked at Landau-Zener-Stuckelberg interferometry (LZS interferometry).

We then used these methods to propose a magnetometer that uses NV-centers in diamonds. We first proposed a method inspired by LZS interferometry, initializing the system in the lower of the three levels and then driving this through the two others, waiting for some time, and then driving it back down again. Picking up Stückelberg phases along the way, that depend on the splitting of the two upper levels. While the method was somewhat promising, we saw several problems. One of those were that driving the levels directly in the manner need was not possible. We therefor had to introduce photon-assisted LZT as a way of driving the system, but this introduced oscillations in the system which made the signal noisy. We therefore saw that a single shot measurement was problematic. The analytical treatment does however show the right periodic nature the return probability, it being periodic in the wait time with a frequency corresponding to the level splitting. We then turned our attention to a second proposal that used oscillations in the lower level in an NV-center to induce Rabi oscillations between the two upper levels, a method where the analytic results more closely resembles the simulations. We saw that also here, single shot measurements looks difficult because of the oscillations in the return probability, but in this case we can use the symmetry around resonance to find where the resonance is, with few measurements.

We then turned our attention fully quantum mechanical driving. First introducing a well known model describing a TLS coupled to a photon mode. Then looking at LZT in such systems, both in the case of transverse and longitudinal driving. We compared the two systems, and how it all relates to the semi-classical driving we looked at in the first half of the thesis. To get a better understanding of the system we looked at what would happen if you suddenly

turn on longitudinal driving and also to get an idea of how the model we introduced could be one way to solve classical driving problems. In the end of this part of the thesis we found the general effective coupling between two sidebands $\langle 1, n| H |0, m\rangle$, in the case of longitudinal driving.

For the last part of the thesis investigated how we could run the system through avoided level crossings to manipulate a type of photon state, namely coherent states and a superposition thereof. We looked into how we could turn cat states into other cat states, using both interference effects and adiabatic transfer. Ultimately we proposed a new method of creating cat states from coherent states using photon-assisted Landau-Zener transitions, more specifically using the photon number dependence of the coupling as a key part.

This last part is the most promising for future work as the resulting states have many use cases, while generally being complicated to make with current methods. The idea behind the method presented is relatively simple, but there might be better ways of implementing it than the one we looked at in this thesis. Looking into other driving patterns is therefore something that would be interesting. The interference condition presented in the last section is also something that would be interesting to look closer at since it is more of an estimate at this point.

Appendix A

Schrieffer Wolff transformations

This method uses a perturbation theory to diagonalize a matrix. Consider the Hamiltionan on the form $H = H_0 + V$, Where H_0 is block diagonal and all the interaction terms (small) are in V, for the case of two blocks we have:

$$H = \begin{bmatrix} H_1 & V_{12} \\ V_{21} & H_2 \end{bmatrix} \tag{A.1}$$

The idea of the method is introduce some unitary transformation, $U_{SW} = e^S$ that transforms the basis so that the transformed Hamiltonian, $\tilde{H} = e^S(H_0 + \lambda V)e^{-S}$, is block diagonal up to a specified order of a smallness parameter λ. For lower orders it is fairly simple to keep track of the orders of λ and the diagonal/off-diagonal parts, but for a general order we can use projection operators to give us the equations:

$$P_1 \tilde{H} P_2 = 0 \tag{A.2}$$

$$P_2 \tilde{H} P_1 = 0 \tag{A.3}$$

Where P_1 is the projection operator for the upper left part, and P_2 is for the lower right. These equations enforce the vanishing of all off-diagonal parts. We also have to require that $S^\dagger = -S$ for unitarity, but in the case of a real Hamiltonian we can assume the transformation is also real, which implies $S^T = -S$. Since V is small we can also assume S to be, and it depends on elements of the Hamiltonian and can therefor in principle have contributions of different orders in λ as well. So we write:

$$S = \sum_{n=1}^{\infty} \lambda^n S_n. \tag{A.4}$$

$$e^S = \sum_{k=0}^{\infty} \frac{1}{k!} S^k \tag{A.5}$$

$$e^S \approx \sum_{k=0}^{N} \frac{1}{k!} [\sum_{n=1}^{N} \lambda^n S_n]^k \tag{A.6}$$

You can use the projection operator equations and unitary condition to make a set of equation for terms of the same order in λ. You start with lowest order ($\propto \lambda$) to find S_1, then you can use the second order equations and the lower order result to find S_2 and so on.

A.1 By hand

Now let us look at the lowest order result and keep track of everything by hand.

$$\begin{aligned}\tilde{H} &= (1 + S_1 + S_2 + \frac{1}{2}(S_1)^2 + \dots)(H_0 + V)(1 - S_1 - S_2 + \frac{1}{2}S_1^2 + \dots) \\ &= H_0 + V + [S_1, H_0] + [S_1, V] + [S_2, H_0] + \frac{1}{2}[S_1, [S_1, H_0]] + \frac{1}{2}[S_1, [S_1, H_0]] + \dots\end{aligned} \tag{A.7}$$

$[S_1, H_0]$ is of diagonal and of first order, the only term that can cancel this is V, so we get that $[S_1, H_0] = -V$. Inserting this into eq. (A.7), we can figure out the second order result:

$$\tilde{H} = H_0 + [S_2, H_0] + \frac{1}{2}[S_1, V] + \mathcal{O}(\lambda^3) \tag{A.8}$$

From this we see that $S_2 = 0$, since there are no other terms that can cancel the off-diagonal $[S_2, H_0]$ term. We get the second-order result:

$$\tilde{H} = H_0 + \frac{1}{2}[S_1, V] + \mathcal{O}(\lambda^3) \tag{A.9}$$

Where S_1 is such that:

$$[S_1, H_0]_{ij} = -V_{ij} \implies (S_1)_{ij} = \frac{V_{ij}}{E_i - E_j} \tag{A.10}$$

And the correction to H_0 is:

$$\frac{1}{2}[S_1, V]_{ij} = \frac{1}{2}\left(\frac{V_{ik}V_{kj}}{E_i - E_k} - \frac{V_{ik}V_{kj}}{E_k - E_j}\right) \tag{A.11}$$

$$\frac{1}{2}[S_1, V]_{ii} = \left(\frac{V_{ik}V_{ki}}{E_i - E_k}\right) \tag{A.12}$$

Which is the result we expect for the second order correction to the energy E_i. Higher order corrections can be found in the same way as we have done here, using of diagonal elements to cancel other of diagonal elements while using lower order results.

Appendix B

Simulations

In this appendix we present examples of codes for the two main types of simulation we have done. For the classical driving we show the code from the indirect Rabi oscillations simulations, while for the fully quantum mechanical driving we show the example of a TLS longitudinally coupled to a bosonic mode with a linearly driven level splitting.

B.1 classical driving

```
import numpy as np
from qutip import *

#make names for the basis functions
one = basis(3,0)
two = basis(3,1)
three = basis(3,2)

#Initial and end state
psi0  = three
psiEnd = three

#Hamiltonian
ofDiagH1 = one*three.dag() * d + two*three.dag()*d
ofDiagH = ofDiagH1 + ofDiagH1.dag()
H0 = -two*two.dag()*E - three*three.dag()*e +ofDiag
H1 = A*three*three.dag()
H = [H0,[H1,H1_coeff]]

def H1_coeff (t, args):
    tau = args['tau']
    linearDriving = (e- w0 + xi)/(2*alpha)
    tp = t-(linearDriving+ tau))
    if (t < linearDriving):
        return np.sin((w0 + alpha * t)*t)
    elif (t>=linearDriving and t<=(linearDriving + tau)):
        return np.sin(w*t)
    elif (t>(linearDriving+tau)):
        return np.sin(((w0 + linearDriving*2*alpha)- alpha*(tp))*(tp))

result = mesolve(H, psi0, t_list, args={'tau': tau})
```

B.2 Fully QM Hamiltonian

```
import numpy as np
from qutip import *

#Defining new sigma matrixes
sigmah = basis(2,0)* basis(2,0).dag()
sigmal = basis(2,1)* basis(2,1).dag()

#Defining the sigma matrices in the photon x TLS basis
sm = tensor(sigmam(), identity(N))
sp = tensor(sigmap(), identity(N))
sz = tensor(sigmaz(), identity(N))
sx = tensor(sigmax(), identity(N))
sh = tensor(sigmah, identity(N))
sl = tensor(sigmal, identity(N))

#The anihilation operator in our basis
a = tensor(identity(2), destroy(N))

#Hamiltonian
H0 = w0*sh - A*sl*(a + a.dag())+ w*a.dag()*a -sx*g
H1 = -v*sh
H = [H0,[H1,H1_coeff]]

def H1_coeff(t, args):
    return t

#TLS start state
tls0 = basis(2,0)

#coherent states
photon0p = coherent(N,alpha)
photon0m = coherent(N,-alpha)

#times
tlist = np.linspace(0,endT,steps)

#Start state in the photon x TLS basis
psi0 =(tensor(tls0,photon0p) + tensor(tls0,photon0m)).unit()

result = mesolve(H, psi0, tlist)
```

Bibliography

[1] D. Leibfried et al. "Quantum dynamics of single trapped ions". In: *Rev. Mod. Phys.* 75 (1 Mar. 2003), pp. 281–324.

[2] Jan R Rubbmark et al. "Dynamical effects at avoided level crossings: A study of the Landau-Zener effect using Rydberg atoms". In: *Physical Review A* 23.6 (1981), p. 3107.

[3] Marc A Kastner. "Artificial atoms". In: *Physics today* 46 (1993), pp. 24–24.

[4] RC Ashoori. "Electrons in artificial atoms". In: *Nature* 379.6564 (1996), p. 413.

[5] R.P. Feynman et al. *The Feynman Lectures on Physics; Vol. 3*. Basic Books, 2011.

[6] Kejie Fang et al. "High-Sensitivity Magnetometry Based on Quantum Beats in Diamond Nitrogen-Vacancy Centers". In: *Phys. Rev. Lett.* 110 (13 Mar. 2013), p. 130802.

[7] John JL Morton et al. "Solid-state quantum memory using the 31 P nuclear spin". In: *Nature* 455.7216 (2008), p. 1085.

[8] L. Childress et al. "Coherent Dynamics of Coupled Electron and Nuclear Spin Qubits in Diamond". In: *Science* 314.5797 (2006), pp. 281–285. ISSN: 0036-8075.

[9] M. V. Gurudev Dutt et al. "Quantum Register Based on Individual Electronic and Nuclear Spin Qubits in Diamond". In: *Science* 316.5829 (2007), pp. 1312–1316. ISSN: 0036-8075.

[10] S.N. Shevchenko, S. Ashhab, and Franco Nori. "Landau-Zener-Stückelberg interferometry". In: *Physics Reports* 492.1 (2010), pp. 1–30. ISSN: 0370-1573.

[11] S. Ashhab, J. R. Johansson, and Franco Nori. "Decoherence in a scalable adiabatic quantum computer". In: *Phys. Rev. A* 74 (5 Nov. 2006), p. 052330.

[12] Guozhu Sun et al. "Population inversion induced by Landau–Zener transition in a strongly driven rf superconducting quantum interference device". In: *Applied Physics Letters* 94.10 (2009), p. 102502.

[13] Clarence Zener and Ralph Howard Fowler. "Non-adiabatic crossing of energy levels". In: *Proceedings of the Royal Society of London. Series A, Containing Papers of a Mathematical and Physical Character* 137.833 (1932), pp. 696–702.

[14] L. D. Landau. “Zur Theorie der Energieubertragung II”. In: *Z. Sowjetunion* 2 (1932), pp. 46–51.

[15] Ernst Karl Gerlach Stückelberg. *Theorie der unelastischen Stösse zwischen Atomen*. Birkhäuser, 1933.

[16] Ettore Majorana. “Atomi orientati in campo magnetico variabile”. In: *Il Nuovo Cimento (1924-1942)* 9.2 (Feb. 1932), pp. 43–50. ISSN: 1827-6121.

[17] David Griffiths. *Introduction of Quantum Mechanics*. Prentice Hall, Inc., 1995.

[18] Curt Wittig. “The Landau-Zener Formula”. In: *The Journal of Physical Chemistry B* 109.17 (2005). PMID: 16851989, pp. 8428–8430.

[19] Le Tuan Anh Ho and Liviu F. Chibotaru. “A simple derivation of the Landau-Zener formula”. In: *Phys. Chem. Chem. Phys.* 16 (15 2014), pp. 6942–6945.

[20] A. Zenesini et al. “Time-Resolved Measurement of Landau-Zener Tunneling in Periodic Potentials”. In: *Phys. Rev. Lett.* 103 (9 Aug. 2009), p. 090403.

[21] J.R. Johansson, P.D. Nation, and Franco Nori. “QuTiP: An open-source Python framework for the dynamics of open quantum systems”. In: *Computer Physics Communications* 183.8 (2012), pp. 1760–1772. ISSN: 0010-4655.

[22] J.R. Johansson, P.D. Nation, and Franco Nori. “QuTiP 2: A Python framework for the dynamics of open quantum systems”. In: *Computer Physics Communications* 184.4 (2013), pp. 1234–1240. ISSN: 0010-4655.

[23] Marcus W. Doherty et al. “The nitrogen-vacancy colour centre in diamond”. In: *Physics Reports* 528.1 (2013). The nitrogen-vacancy colour centre in diamond, pp. 1–45. ISSN: 0370-1573.

[24] L Rondin et al. “Magnetometry with nitrogen-vacancy defects in diamond”. In: *Reports on Progress in Physics* 77.5 (May 2014), p. 056503.

[25] Gopalakrishnan Balasubramanian et al. “Ultralong spin coherence time in isotopically engineered diamond”. In: *Nature materials* 8.5 (2009), p. 383.

[26] JM Taylor et al. “High-sensitivity diamond magnetometer with nanoscale resolution”. In: *Nature Physics* 4.10 (2008), p. 810.

[27] JR Maze et al. “Nanoscale magnetic sensing with an individual electronic spin in diamond”. In: *Nature* 455.7213 (2008), p. 644.

[28] C. L. Degen. “Scanning magnetic field microscope with a diamond single-spin sensor”. In: *Applied Physics Letters* 92.24 (2008), p. 243111.

[29] Gopalakrishnan Balasubramanian et al. “Nanoscale imaging magnetometry with diamond spins under ambient conditions”. In: *Nature* 455.7213 (2008), p. 648.

[30] Marcus W. Doherty et al. “Electronic Properties and Metrology Applications of the Diamond NV^- Center under Pressure”. In: *Phys. Rev. Lett.* 112 (4 Jan. 2014), p. 047601.

[31] E. T. Jaynes and F. W. Cummings. “Comparison of quantum and semiclassical radiation theories with application to the beam maser”. In: *Proceedings of the IEEE* 51.1 (Jan. 1963), pp. 89–109. ISSN: 0018-9219.

[32] Florian Meier and David D. Awschalom. "Spin-photon dynamics of quantum dots in two-mode cavities". In: *Phys. Rev. B* 70 (20 Nov. 2004), p. 205329.

[33] J. Basset et al. "Single-electron double quantum dot dipole-coupled to a single photonic mode". In: *Phys. Rev. B* 88 (12 Sept. 2013), p. 125312.

[34] Jongmin Lee et al. "Demonstration of the Jaynes-Cummings ladder with Rydberg-dressed atoms". In: *Phys. Rev. A* 95 (4 Apr. 2017), p. 041801.

[35] B. M. Rodríguez-Lara, H. Moya-Cessa, and A. B. Klimov. "Combining Jaynes-Cummings and anti-Jaynes-Cummings dynamics in a trapped-ion system driven by a laser". In: *Phys. Rev. A* 71 (2 Feb. 2005), p. 023811.

[36] Guido Burkard and J. R. Petta. "Dispersive readout of valley splittings in cavity-coupled silicon quantum dots". In: *Phys. Rev. B* 94 (19 Nov. 2016), p. 195305.

[37] Yuan-Chi Yang, S. N. Coppersmith, and Mark Friesen. "Achieving high-fidelity single-qubit gates in a strongly driven silicon-quantum-dot hybrid qubit". In: *Phys. Rev. A* 95 (6 June 2017), p. 062321.

[38] Sang-Kil Son, Siyuan Han, and Shih-I Chu. "Floquet formulation for the investigation of multiphoton quantum interference in a superconducting qubit driven by a strong ac field". In: *Phys. Rev. A* 79 (3 Mar. 2009), p. 032301.

[39] Jiahao Huang et al. "Quantum metrology with spin cat states under dissipation". In: *Scientific reports* 5 (2015), p. 17894.

[40] W. J. Munro et al. "Weak-force detection with superposed coherent states". In: *Phys. Rev. A* 66 (2 Aug. 2002), p. 023819.

[41] T. C. Ralph et al. "Quantum computation with optical coherent states". In: *Phys. Rev. A* 68 (4 Oct. 2003), p. 042319.

[42] Steven J van Enk and Osamu Hirota. "Entangled coherent states: Teleportation and decoherence". In: *Physical Review A* 64.2 (2001), p. 022313.

[43] T. E. Northup and R. Blatt. "Quantum information transfer using photons". In: *Nature Photonics* 8.5 (Apr. 2014), pp. 356–363.

[44] P. T. Cochrane, G. J. Milburn, and W. J. Munro. "Macroscopically distinct quantum-superposition states as a bosonic code for amplitude damping". In: *Phys. Rev. A* 59 (4 Apr. 1999), pp. 2631–2634.

[45] H. Jeong and M. S. Kim. "Efficient quantum computation using coherent states". In: *Physical Review A* 65.4 (Mar. 2002).

[46] John A Vaccaro and DT Pegg. "Wigner function for number and phase". In: *Physical Review A* 41.9 (1990), p. 5156.

[47] Zhe Sun et al. "Photon-assisted Landau-Zener transition: Role of coherent superposition states". In: *Phys. Rev. A* 86 (1 July 2012), p. 012107.

[48] L. Mandel. "Sub-Poissonian photon statistics in resonance fluorescence". In: *Opt. Lett.* 4.7 (July 1979), pp. 205–207.

[49] Dietrich Leibfried et al. "Creation of a six-atom 'Schrödinger cat' state". In: *Nature* 438.7068 (2005), p. 639.

[50] Bastian Hacker et al. “Deterministic creation of entangled atom–light Schrödinger-cat states”. In: *Nature Photonics* 13.2 (2019), p. 110.

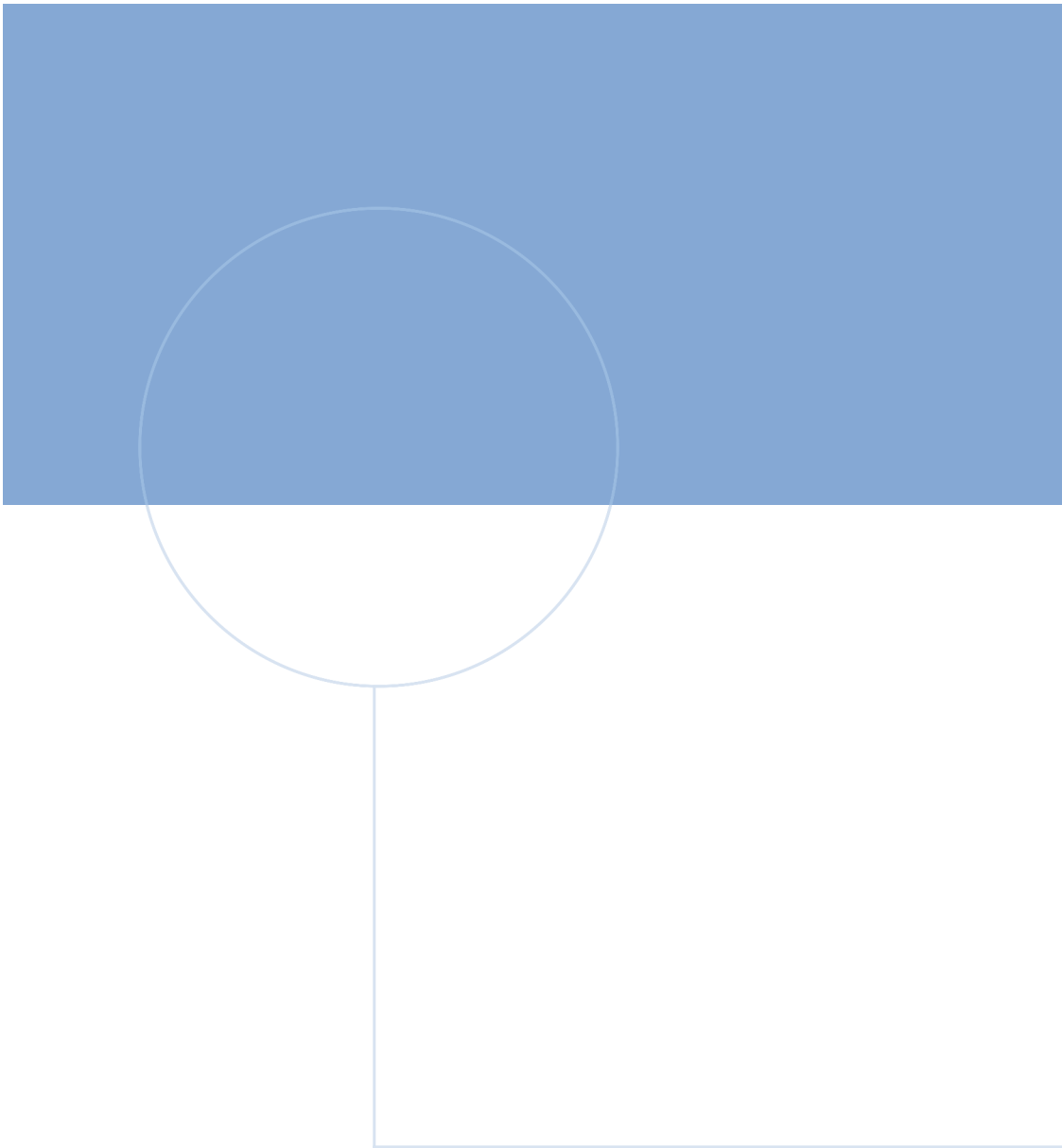

NTNU

Kunnskap for en bedre verden